Department of Biomedical Engineering and Computational Science

Ultra-low-field MRI: techniques and instrumentation for hybrid MEG-MRI

Jaakko Nieminen

Aalto University

DOCTORAL DISSERTATIONS

Aalto University publication series
DOCTORAL DISSERTATIONS 71/2012

Ultra-low-field MRI: techniques and instrumentation for hybrid MEG-MRI

Jaakko Nieminen

Doctoral dissertation for the degree of Doctor of Science in Technology (Doctor of Philosophy) to be presented with due permission of the School of Science for public examination and debate in Auditorium F239 at the Aalto University School of Science (Espoo, Finland) on the 8th of June 2012 at 12 noon.

Aalto University
School of Science
Department of Biomedical Engineering and Computational Science

Supervisor
Prof. Risto Ilmoniemi

Instructor
Prof. Risto Ilmoniemi

Preliminary examiners
Prof. Jens Haueisen, Ilmenau University of Technology, Germany
Prof. Pasi Karjalainen, University of Eastern Finland, Finland

Opponent
Dr. John Mosher, Cleveland Clinic, USA

Aalto University publication series
DOCTORAL DISSERTATIONS 71/2012

ISBN 978-952-60-4644-0 (printed)
ISBN 978-952-60-4645-7 (pdf)
ISSN-L 1799-4934
ISSN 1799-4934 (printed)
ISSN 1799-4942 (pdf)

Unigrafia Oy
Helsinki 2012

Finland

The dissertation can be read at http://lib.tkk.fi/Diss/

441 697
Printed matter

Author
Jaakko Nieminen

Name of the doctoral dissertation
Ultra-low-field MRI: techniques and instrumentation for hybrid MEG-MRI

Publisher School of Science

Unit Department of Biomedical Engineering and Computational Science

Series Aalto University publication series DOCTORAL DISSERTATIONS 71/2012

Field of research Engineering Physics, Biomedical Engineering

Manuscript submitted 28 February 2012 **Manuscript revised** 2 May 2012

Date of the defence 8 June 2012 **Language** English

☐ **Monograph** ☒ **Article dissertation (summary + original articles)**

Abstract

Magnetic resonance imaging (MRI) is a medical imaging modality that can noninvasively produce images of the human body with excellent soft-tissue contrast. Conventionally, MRI is performed in magnetic fields above 1 T. On the other hand, magnetoencephalography (MEG) is a tool for functional brain imaging. In modern MEG, an array of highly sensitive superconducting quantum interference device (SQUID) sensors is used to measure the weak magnetic field around the head produced by neuronal activity in the brain. It has been demonstrated that SQUID sensors can be used to measure also MR signals, if the amplitudes of the MRI fields are reduced and a prepolarization approach is applied. Ultra-low-field (ULF) MRI refers to MRI with signal detection in fields around 100 μT, or even lower, and typically utilizes SQUID sensors for signal readout. The use of the same sensors in MEG and MRI offers significant benefits and allows us to develop a single device capable of both MEG and MRI.

This Thesis introduces several techniques for ULF MRI and its combination with MEG. It is shown that the origin of MR signals can be encoded by preparing the sample consecutively with spatially different polarizing fields. It is also demonstrated that by carefully designing the polarizing-field time course, contrast in ULF MRI can be improved. This Thesis provides also a general method to reconstruct images, when the magnetic fields within the imaging region are nonlinear. In addition, this Thesis describes how to design self-shielded polarizing coils with weak stray fields. Finally, a device for hybrid MEG-MRI was developed based on a commercial whole-head MEG system.

The developed polarization-encoding method may ultimately enable MRI without phase encoding and become essential when developing new kinds of magnetic imaging. The contrast enhancement achieved with time-dependent polarizing fields may be useful when ULF MRI is applied for new purposes. Because in ULF MRI the encoding gradients are relatively strong, conventional reconstruction methods produce image artifacts, whereas the developed general reconstruction method performs much better. The self-shielded polarizing coils are essential when ULF MRI is performed inside magnetically shielded rooms, since otherwise strong eddy currents may be induced in the conductive shielding layers. The developed instrumentation for hybrid MEG-MRI has been successfully used for brain imaging and establishes a solid basis for future research.

Keywords Ultra-low-field MRI, MEG-MRI, magnetic resonance imaging, magnetoencephalography

ISBN (printed) 978-952-60-4644-0 **ISBN (pdf)** 978-952-60-4645-7

ISSN-L 1799-4934 **ISSN (printed)** 1799-4934 **ISSN (pdf)** 1799-4942

Location of publisher Espoo **Location of printing** Helsinki **Year** 2012

Pages 133 **The dissertation can be read at** http://lib.tkk.fi/Diss/

Tekijä
Jaakko Nieminen

Väitöskirjan nimi
Matalakenttä-MRI: menetelmiä ja laitteisto MEG-MRI-kuvantamiseen

Julkaisija Perustieteiden korkeakoulu

Yksikkö Lääketieteellisen tekniikan ja laskennallisen tieteen laitos

Sarja Aalto University publication series DOCTORAL DISSERTATIONS 71/2012

Tutkimusala Teknillinen fysiikka, lääketieteellinen tekniikka

Käsikirjoituksen pvm 28.02.2012 **Korjatun käsikirjoituksen pvm** 02.05.2012

Väitöspäivä 08.06.2012 **Kieli** Englanti

☐ **Monografia** ☒ **Yhdistelmäväitöskirja (yhteenveto-osa + erillisartikkelit)**

Tiivistelmä

Magneettikuvaus (MRI) on lääketieteellinen kuvantamistekniikka, jolla voidaan tuottaa kajoamattomasti kuvia kehosta erinomaisella pehmeän aineen kontrastilla. Tavanomaisesti MRI:ssä käytetään yli 1 T:n magneettikenttiä. Toisaalta magnetoenkefalografia (MEG) on aivojen toimintaa mittaava kuvantamistekniikka. MEG:ssä käytetään erittäin herkkiä suprajohtavia SQUID-sensoreita, joilla aivojen sähköisen toiminnan tuottamaa heikkoa magneettikenttää mitataan pään ulkopuolella. SQUID-sensoreita voidaan käyttää myös MRI:ssä, jos kuvaukseen käytettävien magneettikenttien voimakkuuksia lasketaan. Tällöin kohde on kuitenkin usein esipolarisoitava. Matalakenttä-MRI:ssä MRI-signaaleja mitataan tavanomaisesti SQUID-sensoreilla noin 100 µT:n magneettikentässä. Samojen antureiden käyttäminen MEG:ssä ja MRI:ssä tuo monia etuja ja mahdollistaa yhdistetyn MEG-MRI-laitteen kehittämisen.

Tässä väitöskirjatyössä kehitettiin uusia tekniikoita matalakenttä-MRI:hin ja yhdistettyyn MEG-MRI:hin. Työssä osoitettiin, että MRI-signaalien alkuperä voidaan koodata käyttämällä kuvauskohteen magnetointiin polarisaatiokenttiä, joilla on erilaiset kenttämuodot. Lisäksi työssä osoitettiin, että muotoilemalla polarisaatiokentän aikamuoto sopivasti kuvien kontrastia matalakenttä-MRI:ssä voidaan parantaa. Väitöskirjatyössä kehitettiin myös yleinen kuvanmuodostusmenetelmä, joka toimii silloinkin, kun magneettikentät kuvausalueella vaihtelevat hyvin epälineaarisesti. Lisäksi väitöskirjassa kuvataan, kuinka polarisaatiokelat voidaan suunnitella siten, että niiden tuottama hajakenttä on hyvin pieni. Tässä työssä kehitettiin myös yhdistettyä MEG-MRI-laitetta koko pään kattavan kaupallisen MEG-laitteen pohjalta.

Kehitetty polarisaatiokoodausmenetelmä voi mahdollistaa MRI:n ilman vaihekoodausta ja olla olennaisessa osassa, kun uusia magneettisia kuvausmenetelmiä kehitetään. Optimoiduilla polarisaatiokentän aikamuodoilla saavutettava hyvä kontrasti voi olla hyödyksi, kun matalakenttä-MRI:tä sovelletaan uusilla alueilla. Koska matalakenttä-MRI:ssä koodausgradientit ovat suhteellisen voimakkaita, tavanomaiset kuvanmuodostusmenetelmät voivat tuottaa kuviin vääristymiä. Työssä kehitetty yleinen kuvanmuodostusmenetelmä vähentää näitä vääristymiä huomattavasti. Polarisaatiokelat, jotka tuottavat vain heikon hajakentän, ovat olennaisia, kun MRI:tä tehdään magneettisesti suojatussa huoneessa, sillä muutoin suojahuoneen johtaviin levyihin voi indusoitua voimakkaita pyörrevirtoja. Työssä kehitettyä MEG-MRI-laitetta on käytetty aivojen kuvantamiseen, ja se antaa vankan pohjan jatkotutkimuksille.

Avainsanat Matalakenttä-MRI, MEG-MRI, magneettikuvaus, magnetoenkefalografia

ISBN (painettu) 978-952-60-4644-0 **ISBN (pdf)** 978-952-60-4645-7

ISSN-L 1799-4934 **ISSN (painettu)** 1799-4934 **ISSN (pdf)** 1799-4942

Julkaisupaikka Espoo **Painopaikka** Helsinki **Vuosi** 2012

Sivumäärä 133 **Luettavissa verkossa osoitteessa** http://lib.tkk.fi/Diss/

Preface

During this thesis project, I have had the privilege to work at Department of Biomedical Engineering and Computational Science (BECS), Aalto University School of Science. In addition, I have enjoyed the opportunity to do research at Physikalisch-Technische Bundesanstalt (PTB), Berlin, Germany, and at G. d'Annunzio University, Chieti, Italy. The research has received funding from the European Community's Seventh Framework Programme (FP7/2007–2013) under Grant Agreement No. 200859, the Finnish Cultural Foundation, the Instrumentarium Science Foundation, and the Emil Aaltonen Foundation.

At BECS, I am grateful to my instructor and supervisor Prof. Risto Ilmoniemi for all his guidance. I acknowledge my colleagues and collaborators for pleasant days at work and thank all my co-authors and the members of the MEGMRI project. I devote special thanks to Panu Vesanen, with whom I have spent countless hours in the lab. I thank Koos Zevenhoven and Juhani Dabek for our many great years. Dr. Juha Simola deserves thanks for giving fascinating history lessons during our days in the lab. I thank also my colleagues at PTB, especially, Prof. Lutz Trahms, Dr. Martin Burghoff, Dr. Stefan Hartwig, and Jens Voigt. I am grateful to Prof. Stefania Della Penna, Dr. Raffaele Sinibaldi, Dr. Cinzia De Luca, Dr. Antonietta Manna, and many others for our sunny months in Chieti.

I thank Prof. Raimo Sepponen, Dr. Ilkka Nissilä, Koos Zevenhoven, Panu Vesanen, and the preliminary examiners, Prof. Jens Haueisen and Prof. Pasi Karjalainen, for their useful feedback on the manuscript.

Finally, I thank my family and friends for their support.

Helsinki, May 2, 2012,

Jaakko Nieminen

Contents

List of Publications

This Thesis consists of an overview and of the following publications, which are referred to in the text by their Roman numerals.

I J. O. Nieminen, M. Burghoff, L. Trahms, and R. J. Ilmoniemi. Polarization encoding as a novel approach to MRI. *Journal of Magnetic Resonance*, 202, 211–216, February 2010

II J. O. Nieminen and R. J. Ilmoniemi. Solving the problem of concomitant gradients in ultra-low-field MRI. *Journal of Magnetic Resonance*, 207, 213–219, December 2010.

III J. O. Nieminen, J. Voigt, S. Hartwig, H.-J. Scheer, M. Burghoff, L. Trahms, and R. J. Ilmoniemi. Improved contrast in ultra-low-field MRI with time-dependent bipolar prepolarizing fields: theory and NMR demonstrations. Submitted.

IV J. O. Nieminen, P. T. Vesanen, K. C. J. Zevenhoven, J. Dabek, J. Hassel, J. Luomahaara, J. S. Penttilä, and R. J. Ilmoniemi. Avoiding eddy-current problems in ultra-low-field MRI with self-shielded polarizing coils. *Journal of Magnetic Resonance*, 212, 154–160, September 2011.

V P. T. Vesanen*, J. O. Nieminen*, K. C. J. Zevenhoven, J. Dabek, L. T. Parkkonen, A. V. Zhdanov, J. Luomahaara, J. Hassel, J. Penttilä, J. Simola, A. I. Ahonen, J. P. Mäkelä, and R. J. Ilmoniemi. Hybrid ultra-low-field MRI and MEG system based on a commercial whole-head neuromagnetometer. Submitted.

*These authors contributed equally to this work.

Author's Contribution

Publication I: "Polarization encoding as a novel approach to MRI"

The author invented[1] the method, performed the simulations, and interpreted the results. He is the principal writer of the article.

Publication II: "Solving the problem of concomitant gradients in ultra-low-field MRI"

The author is a co-inventor of the method.[2] He performed the simulations and interpreted the results. He is the principal writer of the article.

Publication III: "Improved contrast in ultra-low-field MRI with time-dependent bipolar prepolarizing fields: theory and NMR demonstrations"

The author developed the theory, performed the simulations, and interpreted the results. He wrote the first version of the manuscript and edited the final version based on the input from the other authors.

---

[1] J. O. Nieminen. Menetelmä, laitteisto ja tietokoneohjelmatuote kohteiden magneettiseksi kuvantamiseksi. Finnish Patent No. 121899, May 31, 2011. [English translation: Method, apparatus, and a computer program for magnetic imaging of samples]

[2] J. O. Nieminen and R. J. Ilmoniemi. Kuvanmuodostusmenetelmä ultramatalakenttäiseen magneettikuvaukseen. Helsinki University of Technology, Intellectual property ID 723, November 11, 2009. [English translation: Reconstruction method for ultra-low-field magnetic resonance imaging]

Publication IV: "Avoiding eddy-current problems in ultra-low-field MRI with self-shielded polarizing coils"

The author is a co-inventor of the method.[3] He developed the theory, performed the simulations, and interpreted the results. He designed the experiments together with the second author. He is the principal writer of the article.

Publication V: "Hybrid ultra-low-field MRI and MEG system based on a commercial whole-head neuromagnetometer"

The author participated in nearly all stages of the development and testing of the instrumentation including experimental and theoretical work. He was the main designer of the coils and support structures. He was one of the main designers and performers of experiments and data analysis. The author was one of the main writers of the manuscript and was responsible for writing the MRI-hardware section. He shares the first authorship.

[3]J. O. Nieminen, P. T. Vesanen, K. C. J. Zevenhoven, and R. J. Ilmoniemi. System and method for prepolarizing magnetic resonance- or relaxation-based measurements. Patent pending, PCT/FI2011/050367, filed April 21, 2011.

List of Abbreviations

DC	Direct current
DNI	Direct neuronal imaging
fMRI	Functional MRI
FOV	Field of view
MEG	Magnetoencephalography
MRI	Magnetic resonance imaging
MSR	Magnetically shielded room
NMR	Nuclear magnetic resonance
NQR	Nuclear quadrupole resonance
pMRI	Parallel MRI
SNR	Signal-to-noise ratio
SQUID	Superconducting quantum interference device
ULF MRI	Ultra-low-field MRI

1. Aims of the Study

The aims of Publications I–V were as follows.

I To develop a new encoding method for prepolarized ultra-low-field magnetic resonance imaging (ULF MRI).

II To develop a general MRI reconstruction method that can handle strong concomitant gradients.

III To demonstrate that optimized time-dependent polarizing fields can improve contrast in ULF MRI.

IV To design a coil that produces a strong polarizing field and, when pulsed, induces only weak eddy currents in the conductive environment, especially in the walls of the magnetically shielded room (MSR) surrounding the system.

V To develop instrumentation for combined magnetoencephalography (MEG) and MRI and to compare its performance against conventional high-field MRI and MEG.

2. Introduction

When matter is subject to an external magnetic field, spins of nuclei with nonzero angular momentum, *e.g.,* hydrogen, align along the field [1]. This polarization leads to macroscopic nuclear magnetization that can be measured with appropriate instrumentation [2–7]. Out of the various measurement paradigms, the most significant impact on imaging has been the combination of nuclear magnetic resonance (NMR) and inductive signal detection [7–9]. In the 1970s, it lead to MRI [10].

MRI is a powerful tool for clinical diagnostics, as it can noninvasively produce images of the human body with excellent soft-tissue contrast. The number of MRI scanners and studies in the world have increased year by year. In 2007, there were about 8000 MRI units only in the USA; 27.5 million examinations were carried out with these scanners [11]. Also the main-field strength of the scanners has increased from the early years of MRI: 1.5-T scanners have been in routine use for many years and 3-T units are becoming increasingly common; currently, an 11.7-T scanner for whole-body imaging is under construction [12]. The pursuit of higher field strengths has been motivated by the increasing image signal-to-noise ratio (SNR).

After the detection of NMR with induction coils was well established, several researchers developed equipment to measure NMR and related phenomena, such as nuclear quadrupole resonance (NQR), with superconducting detectors [13–27]. In the 1990s, it was demonstrated that induction coils in MRI can be replaced with highly sensitive superconducting quantum interference device (SQUID) sensors [28–36]. When combined with sample prepolarization [37] in a field on the order of 10–100 mT, SQUID sensors allows us to reduce the main-field strength and to perform MRI in fields which are as weak as 10–100 μT with reasonable image quality [38, 39]. ULF MRI refers to this kind of MRI, comprising signal

detection in fields around 100 μT, or even lower.

SQUID sensors are used also in biomagnetic measurements. For example in magnetocardiography, the magnetic field arising from the heart is measured outside the body [40]. In MEG, brain function is studied by measuring the magnetic field caused by neuronal activity [41, 42]. The use of the same sensors in MEG and MRI offers significant benefits and allows us to develop a single device for MEG and MRI.

The main goal of this Thesis was to enhance ULF MRI and, in particular, to develop a hybrid device for combined MEG-MRI. I will describe our MEG-MRI instrumentation and show results obtained with it. In addition, I will provide solutions to several fundamental issues that have troubled the field already for some time. I will also introduce unique measurement paradigms that are unreachable in conventional high-field MRI. When applied properly, they may provide additional information about nature by means of novel experiments. A significant amount of work was devoted to studying various aspects of the polarizing field unique to ULF MRI.

3. Background and Methods

In this chapter, MRI is presented in some detail. We will first go through physical principles of MRI and have a glance at conventional MRI. Then, we will familiarize ourselves with ULF MRI. At the end of the chapter, I will also give a brief introduction to MEG.

3.1 MRI physics

MRI is based on NMR, which is intrinsically a quantum-mechanical phenomenon and relates to the spins of nuclei with nonzero spin angular momentum [1]. When matter is subjected to an external magnetic field $\vec{B}$, the spins can align either parallel or anti-parallel to the field. Because it is energetically favorable for the nuclear spins, in thermal equilibrium, a small majority of the spins in matter align parallel to the field, which leads to macroscopic magnetization. This magnetization is proportional to the external magnetic field. If the magnetization is not parallel to $\vec{B}$, it precesses about the field. This precession occurs at the Larmor frequency

$$\vec{\omega}_{\mathrm{L}} = -\gamma \vec{B} \,, \tag{3.1}$$

where γ is the gyromagnetic ratio (for ^{1}H, $\gamma/2\pi = 42.58\,\mathrm{MHz/T}$). For high magnetic fields, ω_{L} is in the radio-frequency range.

Next, let us consider relaxation phenomena present in MRI and NMR. The spin–lattice relaxation time T_1 characterizes the speed by which the longitudinal component of the magnetization, *i.e.,* the component parallel to $\vec{B}$, approaches its thermodynamic equilibrium value $\vec{m}^{\mathrm{eq}}$. The T_1 relaxation originates from interactions between the spins and the lattice. The spin–spin relaxation time T_2 characterizes the speed by which the transverse magnetization, *i.e.,* the magnetization component perpendicular to $\vec{B}$, decreases towards its equilibrium value of zero. The T_2 re-

laxation is caused by random fluctuations in local microscopic magnetic fields, which causes neighboring spins to precess at different frequencies, dephasing them. If the external field is inhomogeneous, the dephasing becomes faster, and the relaxation rate $1/T_2$ can be replaced by $1/T_2^*$, with $1/T_2 < 1/T_2^*$, to include also the contribution of the field inhomogeneity.[1] Usually, the two relaxation rates obey the condition $T_2 \leq T_1$ [43].

Generally, substances exhibit T_1 and T_2 dispersions, *i.e.,* field-dependent relaxation rates, and T_1 and T_2 tend to be shorter at lower magnetic fields. The effect of the external field on T_1 and T_2 relaxations can be explained by molecular level dynamics of the interactions of protons [44]. The relaxation dispersion has been studied extensively within a wide range of field values (~200 μT–2 T) both for healthy [45–47] and pathological [48] tissue. Even though the Cole–Cole expression [46] can explain many dispersion data well by its four parameters (basically, the relaxation rates at low- and high-field limits, the transition field amplitude between those values, and the steepness of the transition), some tissues exhibit dispersion curves with finer structures. For example, tissues containing protein have nitrogen cross-relaxation dips in their relaxation curves [46, 49]. Despite the long history of relaxation–dispersion studies, recent findings with water indicate that the relaxation mechanisms at the zero-field limit are still partially unknown [50].

The combined effect of the Larmor precession and the relaxation of the magnetization $\vec{m}$ can be described by the Bloch equation [8, 51, 52]:

$$\frac{d\vec{m}}{dt} = \gamma\vec{m} \times \vec{B} - \frac{(\vec{m} \cdot \vec{B})\vec{B}}{B^2}\left(\frac{1}{T_1} - \frac{1}{T_2}\right) + \frac{\vec{m}^{\mathrm{eq}}}{T_1} - \frac{\vec{m}}{T_2}\,, \tag{3.2}$$

where t is time and, on the right-hand side, the first term accounts for the Larmor precession and the others describe the relaxation phenomena. Note that $\vec{m}^{\mathrm{eq}} \propto \vec{B}$. Eq. (3.2) tells us how the magnetization evolves during MRI experiments. The time-dependent magnetization produces a magnetic field, which can be measured outside the sample. From the measured signals, MR images can be reconstructed.

[1] The use of T_2^* is typically only an approximation; the precise signal characteristics depend on the magnetic field distribution within the sample. If the magnetic field amplitude within the sample follows the Lorentz distribution, $1/T_2^* = 1/T_2 + 1/T_2^\dagger$, where $1/T_2^\dagger$ gives the contribution of the field inhomogeneity [1].

3.2 Conventional MRI

MRI is a noninvasive method used to produce images of the interior structure of matter. Compared with other major structural medical imaging technologies, MRI does not include ionizing radiation in contrast to computed tomography [53] and does not suffer from poor penetration through bones as does ultrasound imaging [54].

Because the sample magnetization and the precession frequency both depend linearly on the magnetic field strength, the induced voltage on a receiving induction coil scales as the square of the field; thus, MRI is commonly performed in fields above 1 T. Such scanners typically require heavy solenoidal superconducting magnets, which make them expensive. Scanners operating at lower fields, say 0.1–1 T, can be made more open and less expensive. However, they suffer from reduced signal strengths.

Regardless of the chosen field strength, a conventional MRI system comprises a homogeneous main field $\vec{B}_0$ pointing in the z direction. This field defines a single Larmor frequency. To encode the spatial origin of the signal, conventional MRI utilizes three linear gradient fields. In the context of MRI, a linear gradient field is a magnetic field whose z component varies linearly in one direction but remains constant along the perpendicular directions. By superposing gradient fields on the main field, the Larmor frequency can be made spatially dependent. Another essential part of MRI systems is an excitation field $\vec{B}_1$ at the Larmor frequency; it is used to reorient the sample magnetization. In MRI, π and $\pi/2$ pulses refer to excitation pulses rotating the magnetization vector by 180° and 90°, respectively. By properly controlling the gradient and excitation fields and by acquiring the respective data with induction coils tuned to the Larmor frequency in $\vec{B}_0$, the origin of the signals can be decoded.

Commonly, signal encoding is done so that the image can be reconstructed by Fourier-transforming the measured data. This can be achieved by applying linear gradient fields during or prior to the signal acquisition so that the phase and the frequency of the MR signal depend linearly on the position [10]. Another group of methods utilizes tailored excitation pulses together with the gradient fields to control the flip angles within the sample, producing spatial magnetization profiles [55, 56]. For example, these methods can produce wavelet-shaped signal profiles, enabling image reconstruction via inverse wavelet transforms. In Publication I, an encoding method based on spatially different polarizing fields is intro-

duced.

The above-mentioned encoding methods require only one receiver channel. Receiver arrays consisting of local coils, however, provide several advantages and can also be used for signal encoding [57, 58]. First, sampling independent information with several coils in parallel can be used to reduce the imaging time [59–67]. The underlying idea of parallel MRI (pMRI) is to acquire less data per channel than what is required to reconstruct the image with a single-channel receiver. By sampling partial data in parallel with sensors having spatially different sensitivity profiles, a full image can be reconstructed. In addition to the improvement in imaging speed, pMRI may also help in reducing image artifacts [68, 69]. Sensor arrays can be used also to enhance the image SNR; a small coil typically picks up less noise from the sample than a large one, which leads to an overall improvement in the image SNR when a combined image is formed [57].

3.3 Ultra-low-field MRI

When the main field is lowered to the level of, say, 100 μT, the signal strength is reduced if the imaging paradigm is left intact. Fortunately, there are several ways to overcome the signal loss at such low field strengths. First, the sample magnetization can be boosted up by several means independently of the main field, *e.g.,* with a polarizing field [37], making the sample magnetization independent of B_0.[2] Second, because the performance of induction coils at low frequencies is poor [76], the MR signals can be recorded with sensors having better sensitivity at those frequencies, *e.g.,* SQUID magnetometers [77]. Third, external magnetic interference can be reduced by providing shielding against it, *e.g.,* by placing the system inside an MSR [78]. Combination of the prepolarization concept with the use of highly sensitive detectors inside a light MSR was demonstrated in NMR and MRI in the early 2000s [38, 79]. These studies marked the beginning of a new era in MRI; they showed that it is possible to image large, room-temperature samples in fields on the order of 100 μT with reasonable image quality. In the following sections, I will introduce different aspects of ULF MRI.

[2] In addition to prepolarization, there are other means to boost MR signal strengths. These include dynamic nuclear polarization [1, 70, 71], which is based on the Overhauser effect [72], and the use of optically pumped noble gases [73–75].

3.3.1 Advantages of ULF MRI

Compared with conventional high-field MRI, ULF MRI has several advantages. Because the broadening of the NMR line width scales linearly with the absolute inhomogeneity of the main field, ULF MRI has less stringent requirements for relative field homogeneity [38, 79]. Although in high-field MRI a sophisticated magnet and a tailored shimming procedure are necessary for sufficient field uniformity, ULF MRI succeeds with much simpler coils. A related advantage of ULF MRI is that susceptibility differences within the sample cause far less distortion than at high fields [74]. Spatial variations in magnetic susceptibility create local magnetic field gradients causing significant NMR line broadening at high magnetic fields; spatially-inhomogeneous broadening may cause image distortions. At low fields, the local field gradients are reduced together with the applied magnetic field strength; thus, susceptibility variations are typically not a problem in ULF MRI. As a consequence, imaging of, *e.g.,* lung and frontal sinuses may be easier at ultra-low fields. In addition, because high-frequency electromagnetic fields penetrate poorly through conductive material, the presence of metal hampers MRI at high fields. In contrast, at ultra-low fields, MR signals can easily be acquired even through metallic cans [80].

Unlike high-field MRI, ULF MRI is silent, as forces on coil structures are weak because of low magnetic fields. In addition, because of the reduced forces, low magnetic fields are safer than high fields, allowing potentially new patient groups, *e.g.,* people with various metallic implants, to enter the scanner. The low field strengths also make it convenient to design ULF-MRI systems with open geometry whereas at high fields, a solenoidal main magnet is typically unavoidable. The overall weight of an ULF-MRI device can be significantly lower than that of a typical high-field-MRI system, facilitating the structural requirements of its location inside buildings.

Low magnetic fields also allow us to build hybrid devices for ULF MRI and MEG [39, 81, 82]. Such devices can then image both the structure and the electrical activity of the brain. At present, precise MEG-data analysis requires that an MR image of the subject is taken with a separate scanner. Problems involved in such workflow include inaccurate co-registration of the MEG and MRI coordinate systems and possible movement and deformation of the brain between the two scans. With a

hybrid MEG-MRI device, the errors related to these inaccuracies are expected to be reduced. In combined MEG-MRI, the additional cost of the MRI part could potentially be only a small fraction of the total cost of the device.

One clear advantage of ULF MRI is also that it is convenient to extend the instrumentation with additional coils. This could be particularly useful for the imaging of current densities or conductivities. By supplying external current through an object, the magnetic field inside the sample changes and depends on the spatial distribution of the current. This change alters the spin dynamics within the object, and, under appropriate conditions, can be seen in the measured MR signals. In high-field MRI, the imaging of static current densities [83–85] requires rotations of the sample, because the system is sensitive only to the changes in the magnetic field component parallel to the static main field. Then again, in ULF MRI, tailored field sequences may allow us to acquire the complete current-density and conductivity information without sample rotations.

The possibility to vary the field strengths can also be utilized with relaxation dispersion to extend the range of different contrasts available in images [86]. The wide contrast palette may prove useful for, *e.g.,* cancer imaging [87–89]. Relaxation dispersion may also help imaging of edemas and internal bleeding, as these change the local relaxation rates. Recently, also interest in security applications of T_1 dispersion has increased [90]; the additional information included in relaxation dispersion may help in discriminating between hazardous and safe liquids. Publication III describes how relaxation dispersion can be utilized to improve image contrast in ULF MRI.

3.3.2 Prepolarization

The use of separate magnetic fields for signal preparation and acquisition was first introduced in the context of NMR experiments in the Earth's field [37]. Since then, the concept has been applied to pulsed-field MRI [91, 92], where the field is first high in order to strongly magnetize the sample and subsequently lowered for signal encoding and acquisition. However, pulsing of a single field does not utilize all the benefits of the prepolarization technique. In principle, the polarizing field can be arbitrarily inhomogeneous as long as its amplitude is sufficiently strong within the whole sample, whereas the main field should typically be much more ho-

mogeneous. Because a coil that produces a uniform field in the target volume is typically less efficient than a coil that produces an inhomogeneous field, the pulsing of a homogeneous field seems suboptimal. Indeed, Ref. [93] describes how a compact polarizing coil can increase the signal strength in MRI with low electrical power.

In principle, the polarizing field can point in any desired direction; however, a common choice so far has been to align it perpendicularly with respect to the main field [87, 94, 95]. This choice has at least one advantage over the others: If the polarizing field is switched off rapidly, *i.e.,* non-adiabatically, the spins remain aligned to the polarizing field and are automatically in the plane transverse to the main field. This means that signal encoding and acquisition can start directly without applying an excitation pulse [37, 95]. However, because the spins will point in the direction of the polarizing field, they memorize the inhomogeneity of the polarizing field. Instead, if the polarizing field is switched off adiabatically in the presence of the main field, after the switching, the alignment of the spins follows the main field. In that case, an excitation pulse is required to initialize precession [94]. The adiabatic switching is useful, as the phase of the magnetization can easily be made equal within the whole sample, and only the amplitude of the magnetization depends on the possible inhomogeneity of the polarizing field. One disadvantage of using a low main field and prepolarization is that when the polarizing field is off, the sample magnetization is not maintained, and a relatively long polarization period is typically needed to reach a sufficient signal strength. Note also that because of the T_1 dispersion, the T_1 relaxation times in the polarizing field tend to be longer the higher the field is, meaning that part of the benefit of using stronger polarizing fields is lost with the need for prolonged polarization periods.

3.3.3 SQUID sensors

Because induction coils perform poorly at low frequencies, ULF MRI at the kilohertz range must utilize more sensitive receivers. So far, the typical choice has been direct-current (DC) SQUID sensors.[3] The SQUID is a superconducting loop having two Josephson junctions [77]. When the

[3]Atomic magnetometers [96, 97] offer a cryogen-free alternative for SQUIDs. They have been applied to NMR [98–109] and MRI [110–112]. Mixed sensors [113] based on giant magnetoresistance [114, 115] have also been demonstrated for NMR [116, 117] and MRI [118, 119].

SQUID is biased with a suitable current, the voltage across it depends sinusoidally on the magnetic flux through the loop. The response of the SQUID is linearized by applying a negative feedback that keeps the flux through the loop constant. Commonly, to obtain the best possible energy sensitivity, the SQUID is made small; as such, it is insensitive to magnetic fields. To obtain high field sensitivity, the SQUID is coupled to a superconducting flux transformer, containing basically two loops. A small loop is coupled to the SQUID and the other, called the pickup loop, is made larger. Because the total flux through a superconducting loop is constant, whenever there is a flux through the larger loop, the smaller loop focuses the same flux to the SQUID. Depending on the pickup-loop geometry, the SQUID sensor can be sensitive to the magnetic field amplitude (magnetometers) or its gradients (gradiometers). SQUID sensors are commonly used in biomagnetic applications, *e.g.,* MEG [41].

Superconducting materials can be characterized by their critical temperature T_c, below which their electrical resistivity completely vanishes. If SQUID sensors are fabricated from a material having high enough T_c, they can be operated by immersing them in liquid nitrogen. However, commonly SQUIDs are made using low-T_c superconductors that require cooling by liquid helium. Generally, low-T_c SQUIDs have a better sensitivity than high-T_c SQUIDs; however, they require dewars with better insulation, and thus the gap between the sample and the sensor becomes larger, and part of the benefit is lost. At low frequencies, SQUIDs exhibit $1/f$ noise; above the $1/f$ corner, the noise is white.

One problem with standard SQUID sensors is that they poorly tolerate high magnetic fields and are therefore incompatible with the polarizing field used in ULF MRI; thus, a typical choice has been to place the SQUID inside a superconducting shield that protects it from the external magnetic field [94, 95]. In those implementations, only the pickup loop is directly exposed to the polarizing field. However, the pickup loop may still transmit a strong field to the SQUID. To protect the SQUID also from the indirect field, the input circuit is made resistive during the polarization. This can be achieved by flux dams, or Q-spoilers, which consist of Josephson junctions in series with the loop [21, 120]. When the current in the loop exceeds the critical current of the junction, the junction becomes resistive, preventing the accumulation of a high current. Another alternative is to use cryogenic switches in series with the input circuit [95]. Then, the input loop can be made resistive by activating the heater of

the switch. In our multi-channel ULF-MRI system, we have all-planar SQUID sensors, where the SQUID is located at the center of a planar pickup loop [121]. In the MRI application, the SQUID is protected from the polarizing field by placing niobium plates above and below the SQUID chip and by using flux dams [121]. By this means, we avoid the inconvenience of long twisted cables necessary in the common design where the SQUID is placed inside a superconducting enclosure far from the pickup loop.

3.3.4 Magnetically shielded rooms

When the intrinsic noise of an ULF-MRI system is sufficiently low, the overall noise level can be reduced by providing shielding against environmental noise sources. For ULF MRI at the kilohertz range, a light MSR of an aluminum layer around the measurement system together with gradiometric sensors are enough to render the external magnetic noise insignificant [122, 123]. If ULF MRI is combined with MEG, additional shielding at lower frequencies is usually needed. Such a shielding can be achieved with an MSR consisting of a few layers of mu-metal with high permeability, together with thicker layers of aluminum [124].

However, the presence of a shielded room affects also the imaging. First, pulsing of the magnetic fields inside the MSR induces eddy currents in the conductive layers of the room [123, 125, 126]. These eddy currents create secondary transient magnetic fields that may affect the spin dynamics in the sample or otherwise complicate the imaging, *e.g.,* produce magnetic fields that exceed the dynamic range of the sensors. However, by reducing the conductance of the eddy-current paths [123] or by placing the highly conductive layers behind mu-metal layers [126], the eddy-current problem can be made less severe. Second, if ULF MRI is performed inside a typical MEG-compatible MSR, the presence of mu-metal affects also the DC component of the magnetic fields [125, 126]. In some cases, this may cause undesired magnetic field distortions, which could be avoided, *e.g.,* by taking the presence of the mu-metal into account already when designing the coils. Another approach is to design the coils so that their stray fields are negligible, producing thus nearly equal magnetic fields in free space and inside an MSR. Third, the magnetic materials in the MSR may produce a static remnant field inside the shielded room [127]. Typically, such a field is of low amplitude and can be neglected. On the other hand, it

may affect the imaging, especially if the imaging sequence includes low-amplitude fields. Generally, the potentially harmful effects caused by the shielded room can be minimized by positioning the ULF-MRI system at the center of the MSR. Publication IV shows how MSR problems can be avoided with self-shielded polarizing coils. Similarly, Ref. [128] describes how these problems can be minimized with a self-shielded polarizing coil comprising current loops that are placed close to the MSR walls.

3.3.5 Noise sources

In prepolarized ULF MRI, the imaging time for a given spatial resolution (voxel volume) and SNR is proportional to the square of the noise amplitude. Therefore, the noise level of the system should be as low as possible to obtain high-quality images in a short imaging time. In ULF MRI, noise can be divided into several categories including environmental noise, sensor noise, noise due to current fluctuations in the MRI coils, dewar noise, body noise, and Nyquist noise from the wires of the polarizing coil.

As has been described earlier, environmental noise can be reduced with an MSR and by using gradiometric sensors [122]. Sensor noise depends mainly on the design of the sensor. In some cases, however, the superconducting parts of the sensors that are subject to the polarizing field may trap flux and produce additional noise. Noise current in the MRI coils during the acquisition period may also increase the overall noise level. When applicable, it is thus beneficial to position the sensors so that they are insensitive to, *e.g.,* fluctuations of the the main field. Typically, however, multi-channel systems have sensors in many different orientations, and it may be impossible to avoid the coupling of the noise current to the sensors; thus, the current itself should be made as stable as possible. This can be achieved, *e.g.,* by using batteries as current sources [95] or by filtering the currents obtained from power supplies [87]. In some cases, the noise level can be reduced by using mechanical relays to disconnect all unnecessary coils during the data acquisition [94].

Nyquist noise originating from conductors is a broad category, as, *e.g.,* dewar noise, body noise, and noise from resistive wires all fall into it. If the polarizing coil made of a thick wire is positioned close to the sensors, it may produce a detectable amount of Nyquist noise [129]. Because, for a wire with a given conductive cross-sectional area, the noise spectral density scales as the square of the filament diameter, Litz wire can be used to

reduce the noise below the detection limit [129]. In our system, we use a superconducting polarizing coil, which eliminates the Nyquist-noise problem. By dewar noise I refer to Nyquist noise from the conductive radiation shield, which is used to improve the thermal insulation of the dewar. A common way to reduce the noise from the shield is to make the shield of conductive strips instead of large sheets. Further reduction in the noise level can be achieved by using aluminized polyester fabric [94, 130]. However, these changes also degrade the thermal shielding. Body noise due to tissue conductivity is a significant noise source in high-field MRI [131]. However, because the conductivity of tissues at low frequencies is smaller than at high frequencies [132], with present sensor technology and noise levels, the body noise is invisible in ULF MRI.

3.3.6 Concomitant gradients

One particular feature of ULF MRI is that it is typically necessary to have relatively strong gradient fields. The strength of a gradient field can be characterized by the parameter $\varepsilon = GL/B_0$, where G is the gradient amplitude, L the diameter of the field of view (FOV), and B_0 the main-field strength. In high-field MRI, the main-field and gradient strengths can be, *e.g.,* $B_0 = 3\,\mathrm{T}$ and $G = 30\,\mathrm{mT/m}$, respectively. Within a FOV of diameter $L = 20\,\mathrm{cm}$, these values give $\varepsilon = 2 \cdot 10^{-3}$. By contrast, in ULF MRI the same FOV with $G = 200\,\mu\mathrm{T/m}$ and $B_0 = 50\,\mu\mathrm{T}$ leads to $\varepsilon = 0.8$, indicating that the relative strength of the gradient field is much higher in ULF MRI than in high-field MRI. This poses challenges for the image reconstruction.

Maxwell's equations state that the curl and divergence of a static magnetic field vanish in vacuum. As a consequence, when a magnetic field varies linearly in one direction, concomitant terms arise in the orthogonal dimensions; thus, the treatment of the gradient fields as unidirectional is only an approximation. When the gradient field is much weaker than the main field, however, the transverse components of the field have a minimal effect on the Larmor frequency and the precession axis. Therefore, in high-field MRI, the gradient fields can typically be treated as idealized unidirectional fields and common Fourier-transform reconstruction methods give distortion-free images. On the other hand, in ULF MRI, the presence of the concomitant gradients may cause image artifacts if the reconstruction method neglects them [133–135].

When $\varepsilon < 1$, image artifacts can be corrected by post-processing methods [136, 137]. However, because these methods take into account only the lowest-order effects, they become useless when ε is further increased. When $\varepsilon > 1$, Fourier reconstruction can produce distortion-free images only in special cases [138–141]. Also in high-field MRI, some applications suffer from the concomitant gradients. For example, in phase-contrast MR, axial echo-planar imaging, and fast spin-echo imaging, it may be necessary to modify the pulse sequences and to use improved reconstruction algorithms to avoid the concomitant-gradient artifacts [142–144]. The problem of concomitant gradients is solved in Publication II.

3.3.7 Superconducting polarizing coils

One novelty in our ULF-MRI system is the self-shielded superconducting polarizing coil (see Fig. 3.1). Resistive polarizing coils are typically heavy and large, requiring active cooling to achieve high polarizing-field amplitudes [87, 95]. Furthermore, a large polarizing coil induces strong eddy currents in the conductive environment, especially in the layers of the MSR [126]. To address these problems, our system features a superconducting polarizing coil that has a high filling factor, low weight, and compact design. The superconducting wire in the coil has approximately 24000 Nb filaments (filament size ~1 µm) in a bronze matrix (Supercon, Inc., Boston, MA, USA). The coil is wound around the frame holding the SQUID modules. To minimize the heat production and helium boil-off,

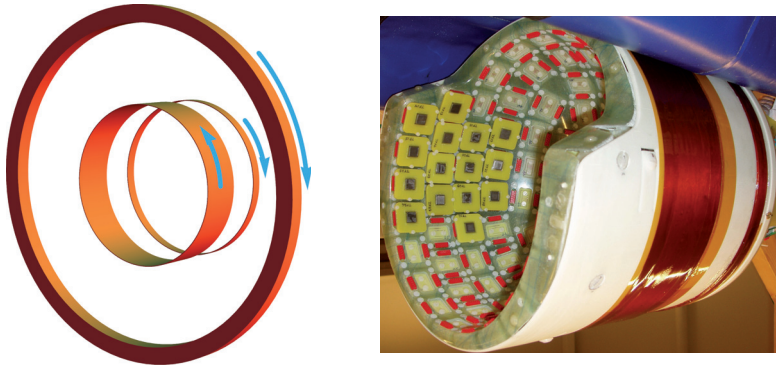

Figure 3.1. Left: A schematic drawing of our self-shielded polarizing coil. The arrows indicate the direction of the current flow in the coils. The small-diameter coils are superconducting and the largest one is made of copper. Right: A photograph of the sensor insert showing the low-T_c superconducting parts of the polarizing coil wound around the frame holding the planar SQUID modules.

the low-T_c coil is connected to high-T_c REPCO leads (SuperPower, Inc., Schenectady, NY, USA) forming the connection up to the neck plug of the dewar. There, they are further connected to brass strips that produce a low-thermal-conductivity path out of the helium space of the dewar.

When choosing wire material for a low-T_c superconducting polarizing coil, there are several issues worth consideration. First, the critical current density of the superconductor should be high enough to permit the current flow. Second, the coil should remain superconducting in relatively strong magnetic fields, ruling out type-I superconductors. Third, the coil should not have a significant remnant magnetization after the polarizing field is turned off; thus, the matrix material should be non-magnetic. In addition, the superconducting filaments should not trap a significant amount of flux. For that reason, the lower critical field of the type-II superconducting filament material should be high to avoid flux trapping at low field values. Additionally, the filament diameter should be small: according to an approximate model for long filaments with circular cross-section in a perpendicular magnetic field, the magnetization depends linearly on the filament thickness [145].

Our polarizing coil produces ~2 mT/A within the imaging volume; however, the field experienced by the superconducting wire material is much stronger. Despite the thin filaments, the coil seemed to trap a significant amount of flux when driven with currents above 12 A. The trapped flux produced a remnant field with large variations within the imaging region. A slight remnant field was already visible after polarization with 1-A current. Even with an 11.7-A pulse, however, the remnant field within the imaging region stayed under 800 nT; furthermore, the component of the field parallel to the main field, *i.e.,* the component with the largest effect on the Larmor frequency, seemed to remain under 400 nT. Because this remnant field varies within the FOV, it introduces an additional gradient field, which affects the spins. The estimated maximum gradient in the z component of the remnant field within the FOV was ~4 μT/m. Thus, if the image reconstruction neglects the presence of the remnant field, small distortions may appear in the image. A more severe problem appeared when the current was increased above 12 A. Within the range 12–27 A, the remnant field after polarization seemed to increase rather linearly as a function of the applied current. After a 27-A pulse, the remnant field on the coil axis varied from −4 μT to 24 μT. This strong field makes traditional MRI reconstruction impractical, as the Larmor frequency within

the sample varies extremely nonlinearly. Thus, at present our polarizing field is limited to being below 24 mT.

The available polarizing-field strength may be increased by designing the coil so that the field the superconducting material experiences is as low as possible. A related problem is present also in high-field MRI, where the magnets have to be designed so that the upper critical field of the superconducting material in the magnet is not exceeded. For example, an 11.7-T magnet can be designed so that the maximum field experienced by the superconducting coil is ca. 12 T [146]. However, to significantly increase the ratio between the polarizing field and the field experienced by the wire material, tailored dewars may be required, as the space available in typical MEG dewars is rather limited.

Another possibility to overcome the limited polarizing-field amplitude may be the addition of cancellation coils that would produce an opposing field for the remnant field. However, it may be difficult to reach a shimming accuracy that allows us to completely neglect the remnant field. Yet another approach might be some kind of a degaussing procedure. In its simplest form, first a polarizing field could be applied in the negative direction, causing flux trapping in the wire. Subsequently, a positive field with a lower amplitude could be applied to expel the vortices. We have already tested this method by degaussing our polarizing coil after a 25-A pulse. However, the applicability of the degaussing depends, *e.g.,* on the shape of the magnetization hysteresis curve and the distribution of magnetic fields affecting the coil. If the remnant field cannot be removed, it should be taken into account in the image reconstruction, *e.g.,* by applying the method of Publication II.

3.3.8 ULF-MRI systems and applications

Since the first NMR studies utilizing prepolarization in the Earth's magnetic field [37], it took some fifty years before SQUID sensors were combined with prepolarization for NMR and MRI [38, 79]. In the last few years, however, interest in ULF MRI has been growing quite rapidly, and several different approaches have emerged. So far, nearly all MRI systems have been single-channel devices [94, 148–153]. However, they typically offer only a small FOV. Despite their limitations, they are suitable for developing and demonstrating new imaging concepts [86, 136, 141]. Single-channel systems have been developed based on both low-T_c [94, 151–153]

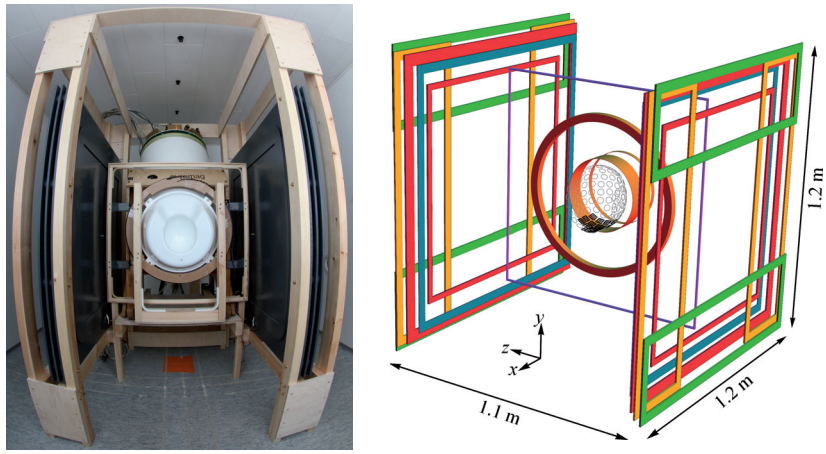

Figure 3.2. Left: A photograph of our system for MEG and ULF MRI without the patient bed [147]. Right: A schematic drawing of the MRI coils and sensors. The main field (red coil) and the gradient fields (G_x: yellow, G_y: green, G_z: blue) are generated by the planar coils on the sides. The polarizing coil (orange) is composed of the three circular coils in the x direction. The small-diameter coils are superconducting and the largest one is made of copper wire. The excitation field is generated by a square coil (purple). The sensor positions are shown in black (in use) and gray (optional).

and high-T_c [148–150] SQUIDs. Although low-T_c SQUIDs offer superior sensitivity, high-T_c SQUIDs have the advantage of cheaper and simpler cryogenics. Refs. [95, 154] describe a 7-channel low-T_c SQUID system for ULF MRI. This multi-channel system has a wide FOV and can be used to image large samples, *e.g.,* the brain [39, 155, 156], with a rather good coverage. Multi-channel ULF-MRI systems may also be applied for pMRI [137]. In Ref. [157], the authors describe their plans to build a SQUID system with 16 ULF-MRI channels and 64 MEG sensors. Our multi-channel instrumentation for hybrid MEG-MRI is described in Publication V.

Fig. 3.2 shows our ULF-MRI system featuring a dewar containing sites for 306 SQUID sensors. Although the design of the polarizing coil and the number of sensors differ substantially from other existing devices, the planar coils for generating the main and gradient fields follow a typical ULF-MRI design. Because MRI is sensitive to absolute inhomogeneity of the main field, even a simple coil can produce a field with a good enough homogeneity when its amplitude is around 10–100 µT. Also, because the gradient strengths in ULF MRI are typically on the order of 100 µT/m, being roughly two orders of magnitude lower than in conventional high-field MRI, the increased inductance of open gradient coils is not limiting

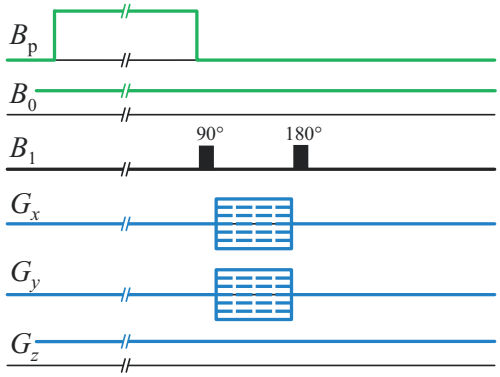

Figure 3.3. A prepolarized 3D spin-echo sequence. At each step, the sample is prepared with the polarizing field $\vec{B}_p$, which is switched off adiabatically. B_0 and B_1 refer to the main and excitation fields, respectively. G_x, G_y, and G_z indicate the encoding gradients.

the system performance.

Fig. 3.3 shows a typical 3D spin-echo sequence with prepolarization. Compared with the respective high-field sequence, there are some differences. First, each step of the sequence starts by applying a polarizing pulse. Second, the frequency-encoding gradient is constantly on, which makes it relatively easy to reach a sufficiently low current-noise level during data acquisition. However, this poses some additional demands for the excitation pulses that have to be able to flip a wide frequency band. Although sinc pulses work reasonably well for the $\pi/2$ pulse, the π pulse is more problematic. If the aim is to excite, *e.g.,* a 1-kHz band uniformly with a sinc pulse, the pulse has to have a flat spectrum over a much wider frequency band. This increases the amplitude of the pulse, if other parameters are held fixed. In high-field MRI, the power of the excitation pulses has to be kept low to guarantee patient safety; therefore, tailored pulse types have been developed to produce good flip-angle uniformity with small pulse amplitudes [158, 159]. These kind of pulses may be useful also for ULF MRI, as they may relax the requirements of the electronics. Note also that because of the low Larmor frequencies, the excitation pulses can easily be driven with power supplies without resonance circuits. The flexibility of ULF-MRI pulse sequences allows even zero-frequency excitation pulses. If the main field is momentarily switched off, excitation pulses could be produced simply by applying a static field of a short duration perpendicularly to the main-field direction, as has been demonstrated in NQR [160] and NMR [22]. This technique can be used to make excitation pulses shorter.

ULF MRI has also been adapted for security applications [90, 161]. Because of the light device weight and low magnetic fields involved, ULF MRI may be useful for screening liquid explosives at airports [90, 161]. The additional information included in the relaxation dispersion of different substances may offer good means for discrimination between safe and dangerous materials [90]. Before being widely usable, there is still a need to improve the scanning speed, as the demonstrated imaging times for small samples have been over one minute [90].

As was briefly mentioned in Section 3.3.1, ULF MRI may be better suited for current-density imaging, as it is convenient to produce nearly arbitrary magnetic field sequences. The conductivity information available from such studies could significantly improve the localization of activated brain regions in hybrid MEG-MRI by providing a more accurate forward model for MEG. Ultimately, ULF MRI might by suitable for direct neuronal imaging (DNI), *i.e.,* detection of neuronal activity by measuring its direct effect on MR signals [162–169]. In contrast to the indirect observation of brain activity in functional MRI (fMRI) [170], the approach of DNI is based on detecting weak variations in local magnetic fields inside the brain caused by neuronal activity. However, the neuronal magnetic fields are much smaller than the blood-flow-related magnetic field changes present in fMRI, making DNI a highly challenging task. If successful, DNI may offer a possibility for novel studies and reveal accurate information about brain function noninvasively.

3.4 Magnetoencephalography

MEG measures the magnetic field around the head produced by neuronal activity in the brain [41, 42]. Because of extremely weak signals in the femtotesla range, current whole-head MEG devices use SQUID sensors.[4] Although high-T_c SQUIDs have been demonstrated in MEG [150, 173–177], the large number of sensors necessary for accurate source localization have made low-T_c SQUIDs the only practical choice, because the fabrication of high-T_c SQUIDs has been much more difficult. Lately, however, a two-channel system utilizing high-T_c SQUIDs was used for MEG [177];

[4]Remarkably, the first MEG recordings were performed using a copper coil as a sensor [171]. However, when SQUID magnetometers with superior sensitivity became available, they were soon applied to MEG [172].

in the future, high-T_c SQUIDs or atomic magnetometers [178–180] may outperform low-T_c SQUIDs in MEG. One of the main advantages of high-T_c SQUIDs with respect to low-T_c sensors is that the gap between the room-temperature environment and the sensor can be reduced to below 1 mm, increasing the amount of information in the measurements when compared with state-of-the-art low-T_c MEG systems with ~2-cm gaps [177].

In whole-head MEG, the magnetic field is typically sampled with several hundred sensors with a time resolution down to 1 ms and below. The activated brain regions are reconstructed from the measured data by solving an inverse problem. In contrast to MRI, in MEG there is no way to encode the precise spatial origin of the signals. Instead, the sources of the signals are estimated using the spatially different sensitivities of the sensors. It has been estimated that, with present MEG systems, less than 100 different simultaneous sources can be distinguished [181]. To find the sources, constraints are needed to limit the number of unknowns. One typical example is to search for a set of current dipoles in the brain that best explains the measured data [182].

MEG has been extensively used in brain research. Since the 1980s, it has also been used for presurgical localization of epileptic seizures [183, 184]. Another clinical application of MEG is the presurgical evaluation of patients with brain tumors [184]. Typically, the estimated sources are visualized on an MR image, which needs to be acquired separately. The need for two separate devices complicates the workflow and introduces errors. It is expected that a hybrid MEG-MRI device could significantly improve the accuracy of MEG localization and, *e.g.,* reduce the cost of the examinations.

In addition to MEG, several other brain imaging techniques exist. Compared with electroencephalography, which is based on measurement of the electric potential differences on the scalp to sense the neuronal activity of the brain, MEG is typically less sensitive to conductivity differences caused, *e.g.,* by the skull. Another group of techniques image brain activity more indirectly, relying on the hemodynamic response [170, 185, 186]. For example, in fMRI, it is possible to differentiate between the presence of paramagnetic deoxyhemoglobin and diamagnetic oxyhemoglobin via their susceptibility differences, giving a high spatial resolution. However, because the blood-oxygen-level-dependent effect scales with the field strength [187], fMRI requires high field strengths and is incompatible with present ULF-MRI devices.

4. Summary of Publications

This chapter summarizes Publications I–V.

4.1 Publication I: "Polarization encoding as a novel approach to MRI"

In this study, a novel encoding method was developed for MRI. Modern multi-channel SQUID systems contain hundreds of sensors that can be used to localize MR signals even without encoding gradients [188]. However, the achievable reconstruction quality is limited by the sensor array. This study demonstrates that, if the sample is prepared using spatially different polarizing fields before consecutive acquisitions (see Fig. 4.1), the reconstruction quality can be enhanced. The effect can be understood by thinking that each polarizing field effectively modifies the spatial sensitivity profiles of the physical sensors, forming virtual receivers with their own sensitivities. Equivalently, one can think that the various polariz-

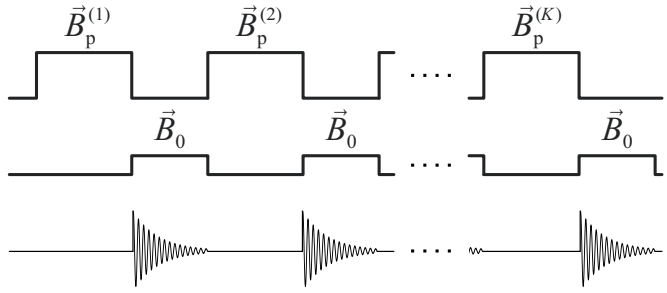

Figure 4.1. A pulse sequence with polarization encoding. Before precession and data acquisition in a homogeneous field $\vec{B}_0$, the sample is polarized using one of the K spatially different polarizing fields $\vec{B}_{\mathrm{p}}^{(i)}$, $i = 1, \ldots, K$. In this sequence, no gradient fields are needed. A modification of the sequence would have a gradient field superposed to $\vec{B}_0$; then, one dimension of the sample would be encoded by the signal frequency.

ing fields dephase the spins in a similar manner as conventional phase-encoding gradients or encoding with excitation pulses. Regardless of the chosen viewpoint, the outcome of the technique is that the number of linearly independent measurements is increased and thus more unknowns can be solved. The results show that by increasing the number of different polarizing fields the image quality is enhanced. Ultimately, the polarization-encoding method might allow MRI without phase encoding, shortening the imaging times.

4.2 Publication II: "Solving the problem of concomitant gradients in ultra-low-field MRI"

This publication provides a general method for reconstructing MR images when the Fourier-transform reconstruction fails. In particular, the study focuses on the problem of concomitant gradients. The publication describes how a general reconstruction matrix can be calculated given the actual magnetic fields. Even in the presence of strong concomitant gradi-

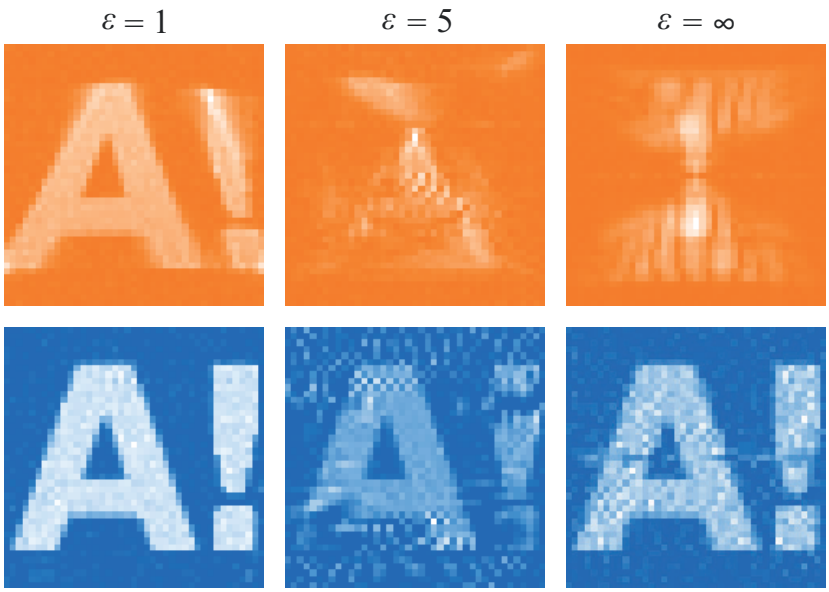

Figure 4.2. Reconstruction results for a simulated phantom containing an "A!"-shaped water structure. A gradient-echo sequence was used with different severity of the concomitant gradients, characterized by the parameter $\varepsilon = GL/B_0$, where G is the maximum gradient strength, L the diameter of the image FOV, and B_0 the strength of the main field. The upper and lower rows show results obtained by Fourier-transforming the simulated data and by using the developed reconstruction method, respectively. For more details, see Publication II.

ents, nearly distortion-free images can be reconstructed by including the concomitant gradients in the reconstruction matrix. The results obtained indicate that the method improves reconstruction quality compared with the Fourier-transform reconstruction (see Fig. 4.2).

4.3 Publication III: "Improved contrast in ultra-low-field MRI with time-dependent bipolar prepolarizing fields: theory and NMR demonstrations"

This study demonstrates how general bipolar and time-dependent polarizing pulses can be used to achieve images with superior contrast. Commonly, the polarizing field in ULF MRI has been considered a field of a fixed amplitude. However, letting it be a function of time expands its applicability (see Fig. 4.3). The publication shows how the polarizing-field time course can be optimized using T_1-dispersion information to maximize the contrast in the final image. The presented concept may be essential when ULF MRI is applied for demanding imaging tasks, *e.g.,* for imaging prostate cancer [88].

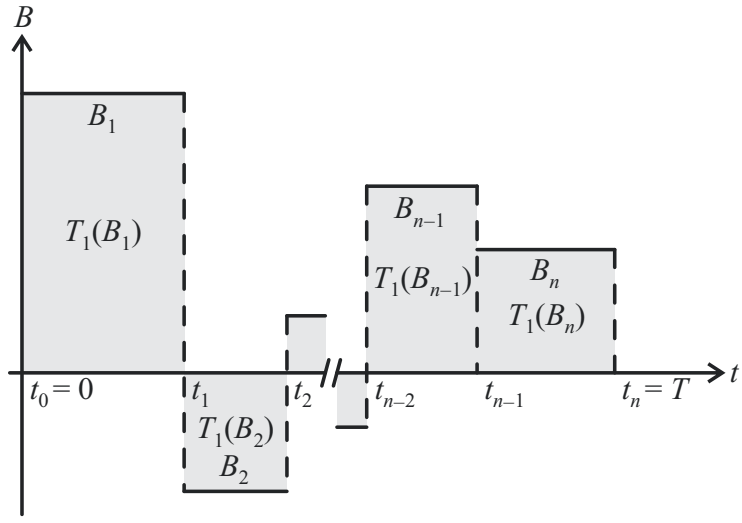

Figure 4.3. The time course of a general bipolar polarizing field. The polarizing field has n steps B_i, $i = 1, \ldots, n$, and the total duration of the pulse is T. During the ith step, the substance to be polarized relaxes according to the relaxation time $T_1(B_i)$.

4.4 Publication IV: "Avoiding eddy-current problems in ultra-low-field MRI with self-shielded polarizing coils"

This study focuses on the eddy-current problem caused by the pulsing of the polarizing field inside an MSR. The publication describes how a polarizing coil can be designed so that its stray field is substantially reduced. Following the instructions in the publication, it is possible to design self-shielded polarizing coils that produce a strong polarizing field but a weak stray field that induces only weak eddy currents; thus, the transient fields within the imaging volume can be made insignificant. One example of such a coil is shown in Fig. 3.1. When the three subcoils are connected in series, the dipole and quadrupole moments of the coil are zero, and the stray field thus decreases rapidly as a function of the distance from the coil. In addition to weakening eddy currents, self-shielded polarizing coils also reduce problems caused by the magnetization of mu-metal layers.

4.5 Publication V: "Hybrid ultra-low-field MRI and MEG system based on a commercial whole-head neuromagnetometer"

This publication describes our instrumentation for MEG and ULF MRI. The multi-channel device is based on a commercial whole-head MEG system by Elekta Oy (Helsinki, Finland). The commercial system includes a helmet-shaped dewar containing 306 planar SQUID sensors arranged in 102 modules each having a magnetometer and two orthogonal planar gradiometers. The MEG-MRI device (see Fig. 3.2) features a self-shielded superconducting polarizing coil and planar SQUID sensors that are protected from the polarizing field by niobium plates and flux dams. The device has been successfully applied for ULF MRI of the human brain (see Fig. 4.4) as well as MEG studies of the visual cortex. The results indicate that despite the modifications necessary for ULF MRI, the MEG performance of the system has not significantly deteriorated. The acquired ULF-MR image shows similar anatomical structures as a high-field-MR image of the same subject.

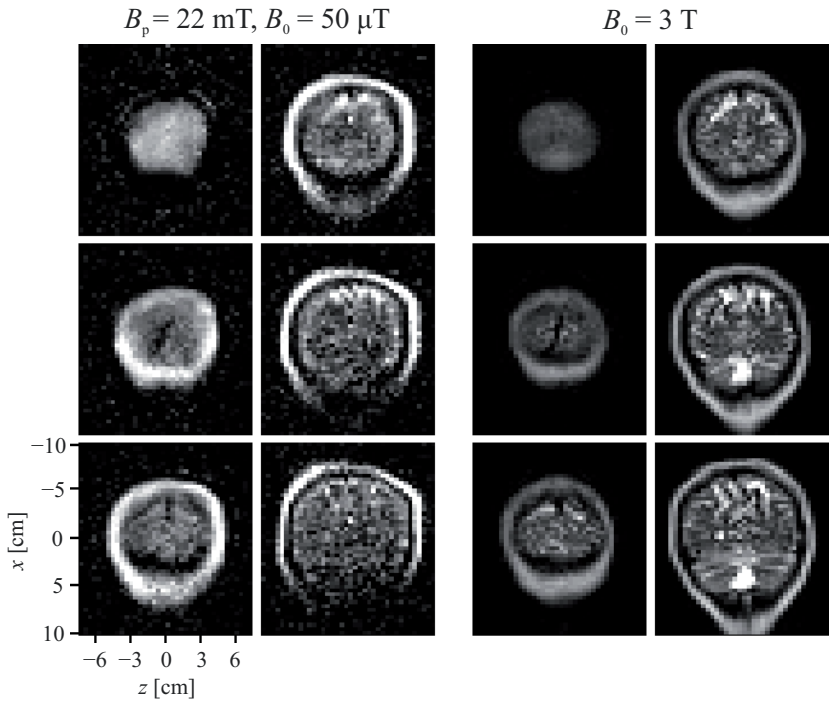

Figure 4.4. Left: Coronal slices of the human brain acquired with the hybrid MEG-MRI device. The polarizing-field and main-field strengths were 22 mT and 50 μT, respectively. The image was acquired with a prepolarized 3D spin-echo sequence with echo time of 122 ms and slice thickness of 6.4 mm. The total imaging time was 92 minutes, involving 8 averages. Right: T_2-weighted high-field-MR image of the same subject obtained at 3 T. The resolution of the high-field-MR image was reduced to match that of the ULF-MR image. For more details, see Publication V.

5. Discussion

This Thesis has introduced new techniques and instrumentation for ULF MRI and its combination with MEG. In addition to ULF MRI, the developed methods may find applications also in other fields. For example, polarization encoding is well suited for applications where frequency and phase-encoding methods are impossible. A recent study demonstrated that the longitudinal proton polarization of a water flow in the absence of precession is measurable by atomic magnetometers [189]. Utilizing the frequency-independent broad-band sensitivity of SQUIDs, it may even be possible to directly measure the relaxation of the longitudinal magnetization of a static sample. Previously, the measurement of the relaxation of magnetic nanoparticles has also been demonstrated in an animal model by using a large sensor array [190] or by moving a sensor with respect to the sample [191]. Together with established reconstruction techniques, polarization encoding may found the basis for a new kind of magnetic imaging.

On the other hand, the reconstruction method of Publication II can be used to reduce distortions caused by arbitrary field inhomogeneities. Currently, we are investigating the possibility to apply the method to correct the distortions caused by the magnetization of the superconducting polarizing coil of our MEG-MRI device. For example, in Fig. 4.4, these distortions are visible as a deformation of the outer surface of the head. However, because with images with a large number of voxels, the computational cost of the method is high, other methods may be more practical with present computers. One way to significantly reduce the computational cost is to handle different Larmor frequencies separately, as was demonstrated recently [192]: First, the measured data are Fourier transformed. For each frequency-encoding step, the transformation defines isofrequency curves. On the other hand, N phase-encoding steps give N

linear equations for each iso-frequency curve. Thus, each iso-frequency curve can be reconstructed separately by solving a small linear inverse problem.

Publication III describes how the polarizing-field time course can be modified to optimize ULF-MR image contrast. By including also T_2 relaxation in the optimization, the method opens new possibilities for improving ULF-MR image quality. The method can be considered a generalization of the inversion-recovery sequence, which is commonly used in high-field MRI to achieve T_1 weighting [193, 194]. Similarly, the method extends the unipolar polarizing-pulse scheme used in Ref. [86] to improve the T_1 weighting of ULF-MR images.

The motivation of self-shielded polarizing coils is similar to that of self-shielded gradient coils, which are used in high-field MRI to reduce eddy-current transients caused by the rapid pulsing of the gradient fields. Self-shielded gradient coils can be designed, *e.g.,* by using Fourier-transform techniques [195–198] or by optimizing the multipole expansion of the coil [199, 200]. However, the field requirements of the gradient and polarizing coils are different. With gradient coils, it is convenient, if the gradient field within the FOV is linear, whereas the precise polarizing-field profile is unimportant as long as the field is sufficiently strong within the FOV. Thus, when designing self-shielded polarizing coils, it is sufficient to concentrate on the multipole expansion of the field outside the coil, with the understanding that the field strength at the FOV per unit current should not decrease too much.

In 2004, simultaneous NMR and MEG recordings with a single-channel system were reported [81]. Thereafter, hybrid MEG-MRI measurements have been demonstrated in consecutive acquisitions [39] and using an interleaved scheme [156] with a 7-channel device. However, to be suitable for advanced MEG studies, an MEG-MRI device should have an extensive sensor array. Currently, our MEG-MRI system has sensors in the region above the occipital lobe; however, we are working to increase sensor coverage. Similarly, other groups are also aiming at whole-head MEG-MRI systems [157]. In addition to providing a larger FOV, whole-head sensor coverage would enhance MR image quality, especially in the deeper regions of the brain [201].

6. Conclusion

This Thesis has provided new tools to enhance ULF MRI and its image quality, bringing us closer to clinically significant imaging. In addition, the results remind us to keep our eyes open and to look for the full potential that imaging at ultra-low fields can offer. Although it is wise to be aware of the methods developed for conventional high-field MRI, one should be careful not to let the high-field approaches bias one's view on what is possible. For example, Publications I and III show how a rethinking of the available sequences can be utilized for signal encoding and image improvements.

Despite the effort put into the development of ULF MRI in this Thesis and around the world, ULF MRI and hybrid MEG-MRI still need some years before they can become clinically significant. To achieve sufficient SNR, the polarizing field should be above or close to 100 mT. In addition, devices should comprise an array of robust sensors and have a low overall noise level.

The outcome of this Thesis is most concretely seen in Publication V in the form of a working device suitable for both MEG and ULF MRI. The developed MEG-MRI system establishes a solid basis for future research at Aalto University. The instrumentation allows development and testing of new imaging concepts that may lead to novel diagnostic tools. In the future, the benefits of hybrid MEG-MRI should be experimentally evaluated. When developing new ULF-MRI techniques, *e.g.,* cancer imaging, one should have a good understanding of the relaxation mechanisms involved at different field strengths in the studied substances. The potential of ULF MRI for current-density and conductivity imaging seems also a promising path when searching for future applications.

Bibliography

[1] A. Abragam. *The Principles of Nuclear Magnetism*. Clarendon Press, Oxford, UK, 1961.

[2] B. G. Lasarew and L. W. Schubnikow. Das magnetische Moment des Protons. *Phys. Zeitschr. Sowjetunion*, 11:445–457, 1937.

[3] I. I. Rabi, J. R. Zacharias, S. Millman, and P. Kusch. A new method of measuring nuclear magnetic moment. *Phys. Rev.*, 53:318, 1938.

[4] I. I. Rabi, S. Millman, P. Kusch, and J. R. Zacharias. The magnetic moments of ${}_3\mathrm{Li}^6$, ${}_3\mathrm{Li}^7$ and ${}_9\mathrm{F}^{19}$. *Phys. Rev.*, 53:495, 1938.

[5] I. I. Rabi, S. Millman, P. Kusch, and J. R. Zacharias. The molecular beam resonance method for measuring nuclear magnetic moments. *Phys. Rev.*, 55:526–535, 1939.

[6] E. M. Purcell, H. C. Torrey, and R. V. Pound. Resonance absorption by nuclear magnetic moment in a solid. *Phys. Rev.*, 69:37–38, 1946.

[7] F. Bloch, W. W. Hansen, and M. Packard. Nuclear induction. *Phys. Rev.*, 69:127, 1946.

[8] F. Bloch. Nuclear induction. *Phys. Rev.*, 70:460–474, 1946.

[9] F. Bloch, W. W. Hansen, and M. Packard. The nuclear induction experiment. *Phys. Rev.*, 70:474–485, 1946.

[10] P. C. Lauterbur. Image formation by induced local interactions: Examples employing nuclear magnetic resonance. *Nature*, 242:190–191, 1973.

[11] OECD Statistics, http://www.oecd.org, May 2, 2012.

[12] P. Vedrine, G. Aubert, F. Beaudet, J. Belorgey, J. Beltramelli, C. Berriaud, P. Bredy, P. Chesny, A. Donati, G. Gilgrass, G. Grunblatt, F. P. Juster, F. Molinie, C. Meuris, F. Nunio, A. Payn, L. Quettier, J. M. Rey, T. Schild, and A. Sinanna. The whole body 11.7 T MRI magnet for Iseult/INUMAC project. *IEEE Trans. Appl. Superond.*, 18:868–873, 2008.

[13] A. H. Silver and J. E. Zimmerman. Multiple quantum resonance spectroscopy through weakly connected superconductors. *Appl. Phys. Lett.*, 10:142–145, 1967.

[14] E. C. Hirschkoff, O. G. Symko, L. L. Vant-Hull, and J. C. Wheatley. Observation of the static nuclear magnetism of pure metallic copper in low magnetic fields. *J. Low Temp. Phys.*, 2:653–665, 1970.

[15] E. P. Day. Detection of NMR using a Josephson-junction magnetometer. *Phys. Rev. Lett.*, 29:540–542, 1972.

[16] D. J. Meredith, G. R. Pickett, and O. G. Symko. Detection of NMR at low temperatures using a superconductive quantum interference device. *Phys. Lett. A*, 42:13–14, 1972.

[17] D. J. Meredith, G. R. Pickett, and O. G. Symko. Application of a SQUID magnetometer to NMR at low temperatures. *J. Low Temp. Phys.*, 13:607–615, 1973.

[18] R. A. Webb. New technique for improved low-temperature SQUID NMR measurements. *Rev. Sci. Instrum.*, 48:1585–1594, 1977.

[19] R. V. Chamberlin, L. A. Moberly, and O. G. Symko. High-sensitivity magnetic resonance by SQUID detection. *J. Low Temp. Phys.*, 35:337–347, 1979.

[20] G. J. Ehnholm, J. P. Ekström, M. T. Loponen, and J. K. Soini. Transversal SQUID NMR. *Cryogenics*, 19:673–678, 1979.

[21] C. Hilbert, J. Clarke, T. Sleator, and E. L. Hahn. Nuclear quadrupole resonance detected at 30 MHz with a dc superconducting quantum interference device. *Appl. Phys. Lett.*, 47:637–639, 1985.

[22] L. J. Friedman, A. K. M. Wennberg, S. N. Ytterboe, and H. M. Bozler. Direct detection of low-frequency NMR using a dc SQUID. *Rev. Sci. Instrum.*, 57:410–413, 1986.

[23] M. R. Freeman, R. S. Germain, and R. C. Richardson. Low-temperature nuclear magnetic resonance with a dc SQUID amplifier. *Appl. Phys. Lett.*, 48:300–302, 1986.

[24] N. Q. Fan, M. B. Heaney, J. Clarke, D. Newitt, L. L. Wald, E. L. Hahn, A. Bielecki, and A. Pines. Nuclear magnetic resonance with DC SQUID preamplifiers. *IEEE Trans. Magn.*, 25:1193–1199, 1989.

[25] N. Q. Fan and J. Clarke. Low-frequency nuclear magnetic resonance and nuclear quadrupole resonance spectrometer based on a dc superconducting quantum interference device. *Rev. Sci. Instrum.*, 62:1453–1459, 1991.

[26] H. C. Seton, D. M. Bussell, J. M. S. Hutchison, I. Nicholson, and D. J. Lurie. DC SQUID-based NMR detection from room temperature samples. *Phys. Med. Biol.*, 37:2133–2138, 1992.

[27] S. Kumar, B. D. Thorson, and W. F. Avrin. Broadband SQUID NMR with room-temperature samples. *J. Magn. Reson. B*, 107:252–259, 1995.

[28] H. C. Seton, D. M. Bussell, J. M. S. Hutchison, and D. J. Lurie. Use of DC SQUID receiver preamplifier in a low field MRI system. *IEEE Trans. Appl. Supercond.*, 5:3218–3221, 1995.

[29] S. Kumar, W. F. Avrin, and B. R. Whitecotton. NMR of room temperature samples with a flux-locked dc SQUID. *IEEE Trans. Magn.*, 32:5261–5264, 1996.

[30] H. C. Seton, J. M. S. Hutchison, and D. M. Bussell. A 4.2 K receiver coil and SQUID amplifier used to improve the SNR of low-field magnetic resonance images of the human arm. *Meas. Sci. Technol.*, 8:198–207, 1997.

[31] H. C. Seton, J. M. S. Hutchison, and D. M. Bussell. A tuned SQUID amplifier for MRI based on a DOIT flux locked loop. *IEEE Trans. Appl. Supercond.*, 7:3213–3216, 1997.

[32] M. P. Augustine, A. Wong-Foy, J. L. Yarger, M. Tomaselli, A. Pines, D. M. TonThat, and J. Clarke. Low field magnetic resonance images of polarized noble gases obtained with a dc superconducting quantum interference device. *Appl. Phys. Lett.*, 72:1908–1910, 1998.

[33] K. Schlenga, R. McDermott, J. Clarke, R. E. de Souza, A. Wong-Foy, and A. Pines. Low-field magnetic resonance imaging with a high-T_c dc superconducting quantum interference device. *Appl. Phys. Lett.*, 75:3695–3697, 1999.

[34] R. E. de Souza, K. Schlenga, A. Wong-Foy, R. McDermott, A. Pines, and J. Clarke. NMR and MRI obtained with high transition temperature DC SQUIDs. *J. Braz. Chem. Soc.*, 10:307–312, 1999.

[35] H. C. Seton, J. M. S. Hutchison, and D. M. Bussell. Gradiometer pick-up coil design for a low field SQUID-MRI system. *Magn. Reson. Mater. Phys.*, 8:116–120, 1999.

[36] K. Schlenga, R. F. McDermott, J. Clarke, R. E. de Souza, A. Wong-Foy, and A. Pines. High-T_c SQUIDs for low-field NMR and MRI of room temperature samples. *IEEE Trans. Appl. Supercond.*, 9:4424–4427, 1999.

[37] M. Packard and R. Varian. Free nuclear induction in the Earth's magnetic field. *Phys. Rev.*, 93:941, 1954.

[38] R. McDermott, S. K. Lee, B. ten Haken, A. H. Trabesinger, A. Pines, and J. Clarke. Microtesla MRI with a superconducting quantum interference device. *Proc. Natl. Acad. Sci. USA*, 101:7857–7861, 2004.

[39] V. S. Zotev, A. N. Matlashov, P. L. Volegov, I. M. Savukov, M. A. Espy, J. C. Mosher, J. J. Gomez, and R. H. Kraus, Jr. Microtesla MRI of the human brain combined with MEG. *J. Magn. Reson.*, 194:115–120, 2008.

[40] I. Tavarozzi, S. Comani, C. Del Gratta, G. L. Romani, S. Di Luzio, D. Brisinda, S. Gallina, M. Zimarino, R. Fenici, and R. De Caterina. Magnetocardiography: Current status and perspectives. Part I: Physical principles and instrumentation. *Ital. Heart J.*, 3:75–85, 2002.

[41] M. Hämäläinen, R. Hari, R. J. Ilmoniemi, J. Knuutila, and O. V. Lounasmaa. Magnetoencephalography—theory, instrumentation, and applications to noninvasive studies of the working human brain. *Rev. Mod. Phys.*, 65:413–497, 1993.

[42] P. Hansen, M. Kringelbach, and R. Salmelin, editors. *MEG: An Introduction to Methods*. Oxford University Press, Oxford, UK, 2010.

[43] P. T. Callaghan. *Principles of Nuclear Magnetic Resonance Mircroscopy*. Clarendon Press, Oxford, UK, 1991.

[44] N. Bloembergen, E. M. Purcell, and R. V. Pound. Relaxation effects in nuclear magnetic resonance absorption. *Phys. Rev.*, 73:679–712, 1948.

[45] P. A. Bottomley, T. H. Foster, R. E. Argersinger, and L. M. Pfeifer. A review of normal tissue hydrogen NMR relaxation times and relaxation mechanisms from 1–100 MHz: Dependence on tissue type, NMR frequency, temperature, species, excision, and age. *Med. Phys.*, 11:425–448, 1984.

[46] S. H. Koenig and R. D. Brown. III Relaxometry of tissue. In R. K. Grupta, editor, *NMR Spectroscopy of Cells and Organisms, Vol. II*, pages 75–114. CRC Press, Boca Raton, FL, 1987.

[47] H. W. Fischer, P. A. Rinck, Y. van Haverbecke, and R. N. Muller. Nuclear relaxation of human brain gray and white matter: Analysis of field dependence and implications for MRI. *Magn. Reson. Med.*, 16:317–334, 1990.

[48] P. A. Bottomley, C. J. Hardy, R. E. Argersinger, and G. Allen-Moore. A review of ^{1}H nuclear magnetic resonance relaxation in pathology: Are T_1 and T_2 diagnostic? *Med. Phys.*, 14:1–37, 1987.

[49] S. E. Ungersma, N. I. Matter, J. W. Hardy, R. D. Venook, A. Macovski, S. M. Conolly, and G. C. Scott. Magnetic resonance imaging with T_1 dispersion contrast. *Magn. Reson. Med.*, 55:1362–1371, 2006.

[50] S. Hartwig, J. Voigt, H.-J. Scheer, H.-H. Albrecht, M. Burghoff, and L. Trahms. Nuclear magnetic relaxation in water revisited. *J. Chem. Phys.*, 135:054201, 2011.

[51] R. S. Codrington, J. D. Olds, and H. C. Torrey. Paramagnetic resonance in organic free radicals at low fields. *Phys. Rev.*, 95:607–608, 1954.

[52] H. C. Torrey. Bloch equations with diffusion terms. *Phys. Rev.*, 104:563–565, 1956.

[53] J. Hsieh. *Computed Tomography: Principles, Design, Artifacts, and Recent Advances*. SPIE, Bellingham, Washington, USA, 2nd edition, 2009.

[54] A. Fenster, D. B. Downey, and H. N. Cardinal. Three-dimensional ultrasound imaging. *Phys. Med. Biol.*, 46:R67–R99, 2001.

[55] J. B. Weaver, Y. Xu, D. M. Healy, and J. R. Driscoll. Wavelet-encoded MR imaging. *Magn. Reson. Med.*, 24:275–287, 1992.

[56] G. P. Zientara, L. P. Panych, and F. A. Jolesz. Dynamically adaptive MRI with encoding by singular value decomposition. *Magn. Reson. Med.*, 32:268–274, 1994.

[57] P. B. Roemer, W. A. Edelstein, C. E. Hayes, S. P. Souza, and O. M. Mueller. The NMR phased array. *Magn. Reson. Med.*, 16:192–225, 1990.

[58] D. J. Larkman and R. G. Nunes. Parallel magnetic resonance imaging. *Phys. Med. Biol.*, 52:R15–R55, 2007.

[59] D. K. Sodickson and W. J. Manning. Simultaneous acquisition of spatial harmonics (SMASH): Fast imaging with radiofrequency coil arrays. *Magn. Reson. Med.*, 38:591–603, 1997.

[60] K. P. Pruessmann, M. Weiger, M. B. Scheidegger, and P. Boesiger. SENSE: Sensitivity encoding for fast MRI. *Magn. Reson. Med.*, 42:952–962, 1999.

[61] W. E. Kyriakos, L. P. Panych, D. F. Kacher, C.-F. Westin, S. M. Bao, R. V. Mulkern, and F. A. Jolesz. Sensitivity profiles from an array of coils for encoding and reconstruction in parallel (SPACE RIP). *Magn. Reson. Med.*, 44:301–308, 2000.

[62] M. A. Griswold, P. M. Jakob, M. Nittka, J. W. Goldfarb, and A. Haase. Partially parallel imaging with localized sensitivities (PILS). *Magn. Reson. Med.*, 44:602–609, 2000.

[63] M. A. Griswold, P. M. Jakob, R. M. Heidemann, M. Nittka, V. Jellus, J. Wang, B. Kiefer, and A. Haase. Generalized autocalibrating partially parallel acquisitions (GRAPPA). *Magn. Reson. Med.*, 47:1202–1210, 2002.

[64] F.-H. Lin, K. K. Kwong, J. W. Belliveau, and L. L. Wald. Parallel imaging reconstruction using automatic regularization. *Magn. Reson. Med.*, 51:559–567, 2004.

[65] M. P. McDougall and S. M. Wright. 64-channel array coil for single echo acquisition magnetic resonance imaging. *Magn. Reson. Med.*, 54:386–392, 2005.

[66] E. N. Yeh, C. A. McKenzie, M. A. Ohliger, and D. K. Sodickson. Parallel magnetic resonance imaging with adaptive radius in k-space (PARS): Constrained image reconstruction using k-space locality in radiofrequency coil encoded data. *Magn. Reson. Med.*, 53:1383–1392, 2005.

[67] F.-H. Lin, L. L. Wald, S. P. Ahlfors, M. S. Hämäläinen, K. K. Kwong, and J. W. Belliveau. Dynamic magnetic resonance inverse imaging of human brain function. *Magn. Reson. Med.*, 56:787–802, 2006.

[68] M. Weiger, K. P. Pruessmann, R. Österbauer, P. Börnert, P. Boesiger, and P. Jezzard. Sensitivity-encoded single-shot spiral imaging for reduced susceptibility artifacts in BOLD fMRI. *Magn. Reson. Med.*, 48:860–866, 2002.

[69] C. Preibisch, U. Pilatus, J. Bunke, F. Hoogenraad, F. Zanella, and H. Lanfermann. Functional MRI using sensitivity-encoded echo planar imaging (SENSE-EPI). *NeuroImage*, 19:412–421, 203.

[70] K. Golman, J. S. Petersson, J.-H. Ardenkjær-Larsen, I. Leunbach, L.-G. Wistrand, G. Ehnholm, and K. Liu. Dynamic in vivo oxymetry using Overhauser enhanced MR imaging. *Magn. Reson. Imaging*, 12:929–938, 2000.

[71] V. S. Zotev, T. Owens, A. N. Matlashov, I. M. Savukov, J. J. Gomez, and M. A. Espy. Microtesla MRI with dynamic nuclear polarization. *J. Magn. Reson.*, 207:78–88, 2010.

[72] A. W. Overhauser. Polarization of nuclei in metals. *Phys. Rev.*, 92:411–415, 1953.

[73] G. Navon, Y.-Q. Song, T. Rõõm, S. Appelt, R. E. Taylor, and A. Pines. Enhancement of solution NMR and MRI with laser-polarized xeon. *Science*, 271:1848–1851, 1996.

[74] C. H. Tseng, G. P. Wong, V. R. Pomoroy, R. W. Mair, D. P. Hilton, D. Hoffmann, R. E. Stoner, F. W. Hersman, D. G. Cory, and R. L. Walsworth. Low-field MRI of laser polarized noble gas. *Phys. Rev. Lett.*, 81:3785–3788, 1998.

[75] H. E. Möller, X. J. Chen, B. Saam, K. D. Hagspiel, G. A. Johnson, T. A. Altes, E. E. de Lange, and H.-U. Kauczor. MRI of the lungs using hyperpolarized noble gases. *Magn. Reson. Med.*, 47:1029–1051, 2002.

[76] W. Myers, D. Slichter, M. Hatridge, S. Busch, M. Mößle, R. McDermott, A. Trabesinger, and J. Clarke. Calculated signal-to-noise ratio of MRI detected with SQUIDs and Faraday detectors in fields from 10 µT to 1.5 T. *J. Magn. Reson.*, 186:182–192, 2007.

[77] J. Clarke and A. I. Braginski, editors. *The SQUID Handbook*. Wiley-VCH Verlag GmbH & Co. KGaA, Weinheim, Germany, 2004.

[78] A. J. Mager. Magnetic shields. *IEEE Trans. Magn.*, MAG-6:67–75, 1970.

[79] R. McDermott, A. H. Trabesinger, M. Mück, A. Pines, and J. Clarke. Liquid-state NMR and scalar couplings in microtesla magnetic fields. *Science*, 295:2247–2249, 2002.

[80] M. Mößle, W. R. Myers, S.-K. Lee, N. Kelso, M. Hatridge, A. Pines, and J. Clarke. SQUID-Detected in vivo MRI at microtesla magnetic fields. *IEEE Trans. Appl. Supercond.*, 15:757–760, 2005.

[81] P. L. Volegov, A. N. Matlachov, M. A. Espy, J. S. George, and R. H. Kraus, Jr. Simultaneous magnetoencephalography and SQUID detected nuclear MR in microtesla magnetic fields. *Magn. Reson. Med.*, 52:467–470, 2004.

[82] A. N. Matlachov, P. L. Volegov, M. A. Espy, R. Stolz, L. Fritzsch, V. Zakosarenko, H.-G. Meyer, and R. H. Kraus, Jr. Instrumentation for simultaneous detection of low field NMR and biomagnetic signals. *IEEE Trans. Appl. Supercond.*, 15:676–679, 2005.

[83] M. L. G. Joy, G. C. Scott, and R. M. Henkelman. In-vivo detection of applied electric currents by magnetic resonance imaging. *Magn. Reson. Imaging*, 7:89–94, 1989.

[84] P. Pešikan, M. L. G. Joy, G. C. Scott, and R. M. Henkelman. Two-dimensional current density imaging. *IEEE Trans. Instr. Meas.*, 39:1048–1053, 1990.

[85] G. C. Scott, M. L. G. Joy, R. L. Armstrong, and R. M. Henkelman. Measurement of nonuniform current density by magnetic resonance. *IEEE Trans. Med. Imaging*, 10:362–374, 1991.

[86] S. K. Lee, M. Mößle, W. Myers, N. Kelso, A. H. Trabesinger, A. Pines, and J. Clarke. SQUID-detected MRI at 132 µT with T_1-weighted contrast established at 10 µT–300 mT. *Magn. Reson. Med.*, 53:9–14, 2005.

[87] S. E. Busch. *Ultra-low field MRI of prostate cancer using SQUID detection*. PhD thesis, University of California, Berkeley, California, USA, 2011.

[88] S. Busch, M. Hatridge, M. Mößle, W. Myers, T. Wong, M. Mück, K. Chew, K. Kuchinsky, J. Simko, and John Clarke. Measurements of T_1-relaxation in ex vivo prostate tissue at 132 µT. *Magn. Reson. Med.*, 67:1138–1145, 2012.

[89] S.-H. Liao, K.-W. Huang, H.-C. Yang, C.-T. Yen, M. J. Chen, H.-H. Chen, H.-E. Horng, and S. Y. Yang. Characterization of tumors using high-T_c superconducting quantum interference device-detected nuclear magnetic resonance and imaging. *Appl. Phys. Lett.*, 97:263701, 2010.

[90] M. Espy, S. Baguisa, D. Dunkerley, P. Magnelind, A. Matlashov, T. Owens, H. Sandin, I. Savukov, L. Schultz, A. Urbaitis, and P. Volegov. Progress on detection of liquid explosives using ultra-low field MRI. *IEEE Trans. Appl. Supercond.*, 21:530–533, 2011.

[91] J. Stepišnik, V. Eržen, and M. Kos. NMR imaging in the Earth's magnetic field. *Magn. Reson. Med.*, 15:386–391, 1990.

[92] A. Macovski and S. Conolly. Novel approaches to low-cost MRI. *Magn. Reson. Med.*, 30:221–230, 1993.

[93] R. Sepponen. Apparatus and method for the examination of properties of an object. US Patent No. 4,906,931, 1990.

[94] R. McDermott, N. Kelso, M. Mößle, M. Mück, W. Myers, B. ten Haken, H. C. Seton, A. H. Trabesinger, A. Pines, and J. Clarke. SQUID-detected magnetic resonance imaging in microtesla magnetic fields. *J. Low Temp. Phys.*, 135:793–821, 2004.

[95] V. S. Zotev, A. N. Matlashov, P. L. Volegov, A. V. Urbaitis, M. A. Espy, and R. H. Kraus, Jr. SQUID-based instrumentation for ultralow-field MRI. *Supercond. Sci. Technol.*, 20:S367–S373, 2007.

[96] D. Budker and M. Romalis. Optical magnetometry. *Nat. Phys.*, 3:227–234, 2007.

[97] J. Kitching, S. Knappe, and E. A. Donley. Atomic sensors — a review. *IEEE Sensors J.*, 11:1749–1758, 2011.

[98] V. V. Yashchuk, J. Granwehr, D. F. Kimball, S. M. Rochester, A. H. Trabesinger, J. T. Urban, D. Budker, and A. Pines. Hyperpolarized xenon nuclear spins detected by optical atomic magnetometry. *Phys. Rev. Lett.*, 93:160801, 2004.

[99] I. M. Savukov and M. V. Romalis. NMR detection with an atomic magnetometer. *Phys. Rev. Lett.*, 94:123001, 2005.

[100] S. Xu, S. M. Rochester, V. V. Yashchuk, M. H. Donaldson, and D. Budker. Construction and applications of an atomic magnetic gradiometer based on nonlinear magneto-optical rotation. *Rev. Sci. Instrum.*, 77:083106, 2006.

[101] I. M. Savukov, S. J. Seltzer, and M. V. Romalis. Detection of NMR signals with a radio-frequency atomic magnetometer. *J. Magn. Reson.*, 185:214–220, 2007.

[102] M. P. Ledbetter, I. M. Savukov, D. Budker, V. Shah, S. Knappe, J. Kitching, D. J. Michalak, S. Xu, and A. Pines. Zero-field remote detection of NMR with a microfabricated atomic magnetometer. *Proc. Natl. Acad. Sci. USA*, 105:2286–2290, 2008.

[103] J. Belfi, G. Bevilacqua, V. Biancalana, S. Cartaleva, Y. Dancheva, K. Khanbekyan, and L. Moi. Dual channel self-oscillating optical magnetometer. *J. Opt. Soc. Am.*, 26:910–916, 2009.

[104] G. Bevilacqua, V. Biancalana, Y. Dancheva, and L. Moi. All-optical magnetometry for NMR detection in a micro-Tesla field and unshielded environment. *J. Magn. Reson.*, 201:222–229, 2009.

[105] M. P. Ledbetter, C. W. Crawford, A. Pines, D. E. Wemmer, S. Knappe, J. Kitching, and D. Budker. Optical detection of NMR J-spectra at zero magnetic field. *J. Magn. Reson.*, 199:25–29, 2009.

[106] N. C. Garcia, D. Yu, and S. Xu. Optical atomic magnetometer at body temperature for magnetic particle imaging and nuclear magnetic resonance. *Opt. Lett.*, 35:661–663, 2010.

[107] D. J. Michalak, S. Xu, T. J. Lowery, C. W. Crawford, M. Ledbetter, L.-S. Bouchard, D. E. Wemmer, D. Budker, and A. Pines. Relaxivity of gadolinium complexes detected by atomic magnetometry. *Magn. Reson. Med.*, 66:605–608, 2011.

[108] T. Theis, P. Ganssle, G. Kervern, S. Knappe, J. Kitching, M. P. Ledbetter, D. Budker, and A. Pines. Parahydrogen-enhanced zero-field nuclear magnetic resonance. *Nat. Phys.*, 7:571–575, 2011.

[109] M. P. Ledbetter, T. Theis, J. W. Blanchard, H. Ring, P. Ganssle, S. Appelt, B. Blümich, and A. Pines D. Budker. Near-zero-field nuclear magnetic resonance. *Phys. Rev. Lett.*, 107:107601, 2011.

[110] S. Xu, V. V. Yashchuk, M. H. Donaldson, S. M. Rochester, D. Budker, and A. Pines. Magnetic resonance imaging with an optical atomic magnetometer. *Proc. Natl. Acad. Sci. USA*, 103:12668–12671, 2006.

[111] S. Xu, C. W. Crawford, S. Rochester, V. Yashchuk, D. Budker, and A. Pines. Submillimeter-resolution magnetic resonance imaging at the Earth's magnetic field with an atomic magnetometer. *Phys. Rev. A*, 78:013404, 2008.

[112] I. M. Savukov, V. S. Zotev, P. L. Volegov, M. A. Espy, A. N. Matlashov, J. J. Gomez, and R. H. Kraus, Jr. MRI with an atomic magnetometer suitable for practical imaging applications. *J. Magn. Reson.*, 199:188–191, 2009.

[113] M. Pannetier, C. Fermon, G. Le Goff, J. Simola, and E. Kerr. Femtotesla magnetic field measurement with magnetoresistive sensors. *Science*, 304:1648–1650, 2004.

[114] M. N. Baibach, J. M. Broto, A. Fert, F. Nguyen Van Dau, F. Petroff, P. Eitenne, G. Creuzet, A. Friederich, and J. Chazelas. Giant magnetoresistance of (001)Fe/(001)Cr magnetic superlattices. *Phys. Rev. Lett.*, 61:2472–2475, 1988.

[115] G. Binasch, P. Grünberg, F. Saurenbach, and W. Zinn. Enhanced magnetoresistance in layered magnetic structures with antiferromagnetic interlayer exchange. *Phys. Rev. B*, 39:4828–4830, 1989.

[116] H. Dyvorne, C. Fermon, M. Pannetier-Lecoeur, H. Polovy, and A.-L. Walliang. NMR with superconducting-GMR mixed sensor. *IEEE Trans. Appl. Superond.*, 19:819–822, 2009.

[117] M. Pannetier-Lecoeur, C. Fermon, H. Dyvorne, J. F. Jacquinot, H. Polovy, and A. L. Walliang. Magnetoresistive-superconducting mixed sensors for biomagnetic applications. *J. Magn. Magn. Mater.*, 322:1647–1650, 2010.

[118] N. Sergeeva-Chollet, H. Dyvorne, H. Polovy, M. Pannetier-Lecoeur, and C. Fermon. Magnetoresistive hybrid sensors for simultaneous low-field MRI and biomagnetic measurements. In S. Supek and A. Sušac, editors, *17th International Conference on Biomagnetism Advances in Biomagnetism - Biomag 2010*, volume 28 of *IFMBE Proceedings*, pages 70–73. Springer Berlin Heidelberg.

[119] N. Sergeeva-Chollet, H. Dyvorne, J. Dabek, Q. Herros, H. Polovy, G. Le Goff, G. Gannies, M. Pannetier-Lecoeur, and C. Fermon. Low field MRI with magnetoresistive mixed sensors. *J. Phys.: Conf. Ser.*, 303:012055, 2011.

[120] R. H. Koch, J. Z. Sun, V. Foglietta, and W. J. Gallagher. Flux dam, a method to reduce extra low frequency noise when a superconducting magnetometer is exposed to a magnetic field. *Appl. Phys. Lett.*, 67:859–862, 1995.

[121] J. Luomahaara, P. T. Vesanen, J. Penttilä, J. O. Nieminen, J. Dabek, J. Simola, M. Kiviranta, L. Grönberg, C. J. Zevenhoven, R. J. Ilmoniemi, and J. Hassel. All-planar SQUIDs and pickup coils for combined MEG and MRI. *Supercond. Sci. Technol.*, 24:075020, 2011.

[122] J. Clarke, M. Hatridge, and M. Mößle. SQUID-detected magnetic resonance imaging in microtesla fields. *Annu. Rev. Biomed. Eng.*, 9:389–413, 2007.

[123] K. Zevenhoven. Solving transient problems in ultra-low-field MRI. Master's thesis, Aalto University, Espoo, Finland, 2011.

[124] D. Cohen. Large-volume conventional magnetic shields. *Rev. Phys. Appl.*, 5:53–58, 1970.

[125] P. T. Vesanen, J. O. Nieminen, J. Dabek, and R. J. Ilmoniemi. Hybrid MEG-MRI: Geometry and time course of magnetic fields inside a magnetically shielded room. In S. Supek and A. Sušac, editors, *17th International Conference on Biomagnetism Advances in Biomagnetism - Biomag 2010*, volume 28 of *IFMBE Proceedings*, pages 78–81. Springer Berlin Heidelberg.

[126] P. T. Vesanen, J. O. Nieminen, K. C. J. Zevenhoven, J. Dabek, J. Simola, J. Sarvas, and R. J. Ilmoniemi. The spatial and temporal distortion of magnetic fields applied inside a magnetically shielded room. *IEEE Trans. Magn.*, 48:53–61, 2012.

[127] F. Thiel, A. Schnabel, S. Knappe-Grüneberg, D. Stollfuß, and M. Burghoff. Demagnetization of magnetically shielded rooms. *Rev. Sci. Instrum.*, 78:035106, 2007.

[128] S.-M. Hwang, K. Kim, C. S. Kang, S.-J. Lee, and Y.-H. Lee. Effective cancellation of residual magnetic interference induced from a shielded environment for precision magnetic measurements. *Appl. Phys. Lett.*, 99:132506, 2011.

[129] W. R. Myers. *Potential applications of microtesla magnetic resonance imaging detected using a superconducting quantum interference device*. PhD thesis, University of California, Berkeley, California, USA, 2006.

[130] H. C. Seton, J. M. S. Hutchison, and D. M. Bussell. Liquid helium cryostat for SQUID-based MRI receivers. *Cryogenics*, 45:348–355, 2005.

[131] O. Ocali and E. Atalar. Ultimate intrinsic signal-to-noise ratio in MRI. *Magn. Reson. Med.*, 39:462–473, 1996.

[132] S. Gabriel, R. W. Lau, and C. Gabriel. The dielectric properties of biological tissues: II. Measurements in the frequency range 10 Hz to 20 GHz. *Phys. Med. Biol.*, 41:2251–2269, 1996.

[133] D. G. Norris and J. M. S. Hutchison. Concomitant magnetic field gradients and their effect on imaging at low magnetic field strengths. *Magn. Reson. Imaging*, 8:33–37, 1990.

[134] D. A. Yablonskiy, A. L. Sukstanskii, and J. J. H. Ackerman. Image artifacts in very low magnetic field MRI: The role of concomitant gradients. *J. Magn. Reson.*, 174:279–286, 2005.

[135] P. L. Volegov, J. C. Mosher, M. A. Espy, and R. H. Kraus, Jr. On concomitant gradients in low-field MRI. *J. Magn. Reson.*, 175:103–113, 2005.

[136] W. Myers, M. Mößle, and J. Clarke. Correction of concomitant gradient artifacts in experimental microtesla MRI. *J. Magn. Reson.*, 177:274–284, 2005.

[137] V. S. Zotev, P. L. Volegov, A. N. Matlashov, M. A. Espy, J. C. Mosher, and R. H. Kraus, Jr. Parallel MRI at microtesla fields. *J. Magn. Reson.*, 192:197–208, 2008.

[138] C. A. Meriles, D. Sakellariou, A. H. Trabesinger, V. Demas, and A. Pines. Zero- to low-field MRI with averaging of concomitant gradient fields. *Proc. Natl. Acad. Sci. USA*, 102:1840–1842, 2005.

[139] C. A. Meriles, D. Sakellariou, and A. H. Trabesinger. Theory of MRI in the presence of zero to low magnetic fields and tensor imaging field gradients. *J. Magn. Reson.*, 182:106–114, 2006.

[140] L.-S. Bouchard. Unidirectional magnetic-field gradients and geometric-phase errors during Fourier encoding using orthogonal ac fields. *Phys. Rev. B*, 74:054103, 2006.

[141] N. Kelso, S.-K. Lee, L.-S. Bouchard, V. Demas, M. Mück, A. Pines, and J. Clarke. Distortion-free magnetic resonance imaging in the zero-field limit. *J. Magn. Reson.*, 200:285–290, 2009.

[142] M. A. Bernstein, X. J. Zhou, J. A. Polzin, K. F. King, A. Ganin, N. J. Pelc, and G. H. Glover. Concomitant gradient terms in phase contrast MR: Analysis and correction. *Magn. Reson. Med.*, 39:300–308, 1998.

[143] X. J. Zhou, Y. P. Du, M. A. Bernstein, H. G. Reynolds, J. K. Maier, and J. A. Polzin. Concomitant magnetic-field-induced artifacts in axial echo planar imaging. *Magn. Reson. Med.*, 39:596–605, 1998.

[144] X. J. Zhou, S. G. Tan, and M. A. Bernstein. Artifacts induced by concomitant magnetic field in fast spin-echo imaging. *Magn. Reson. Med.*, 40:582–591, 1998.

[145] M. N. Wilson. *Superconducting Magnets*. Oxford University Press, Oxford, UK, 1986.

[146] H. Wada, M. Sekino, H. Ohsaki, T. Tisatsune, H. Ikehira, and T. Kiyoshi. Prospects of high-field MRI. *IEEE Trans. Appl. Supercond.*, 20:115–122, 2010.

[147] The author of the photograph is J. Dabek.

[148] H. Dong, Y. Zhang, H.-J. Krause, X. Xie, and A. Offenhäusser. Low field MRI detection with tuned HTS SQUID magnetometer. *IEEE Trans. Appl. Supercond.*, 21:509–513, 2011.

[149] K.-W. Huang, S.-H. Liao, H.-C. Yang, H.-H. Chen, H.-E. Horng, M. J. Chen, and S.-Y. Yang. Low-field nuclear magnetic resonance and magnetic resonance imaging using a high-T_c SQUID for tumor detection. *IEEE Trans. Appl. Supercond.*, 21:461–464, 2011.

[150] F. Öisjöen. *High-T_c SQUIDs for biomedical applications: Immunoassays, MEG, and ULF-MRI*. PhD thesis, Chalmers University of Technology, Gothenburg, Sweden, 2011.

[151] J. Hatta, M. Miyamoto, Y. Adachi, J. Kawai, G. Uehara, and H. Kado. SQUID-based low field MRI system for small animals. *IEEE Trans. Appl. Supercond.*, 21:526–529, 2011.

[152] S. Fukumoto, M. Hayashi, Y. Katsu, M. Suzuki, R. Morita, Y. Naganuma, Y. Hatsukade, S. Tanaka, and O. Snigirev. Liquid-state nuclear magnetic resonance measurements for imaging using HTS-rf-SQUID in ultra-low field. *IEEE Trans. Appl. Supercond.*, 21:522–525, 2011.

[153] I. Hilschenz, R. Körber, H.-H. Albrecht, A. Cassara, T. Fedele, S. Hartwig, H.-J. Scheer, L. Trahms, J. Haase, and M. Burghoff. Magnetic resonance imaging at frequencies below 1 kHz. Submitted.

[154] V. S. Zotev, A. N. Matlachov, P. L. Volegov, H. J. Sandin, M. A. Espy, J. C. Mosher, A. V. Urbaitis, S. G. Newman, and R. H. Kraus, Jr. Multi-channel SQUID system for MEG and ultra-low-field MRI. *IEEE Trans. Appl. Supercond.*, 17:839–842, 2007.

[155] V. S. Zotev, A. N. Matlashov, I. M. Savukov, T. Owens, P. L. Volegov, J. J. Gomez, and M. A. Espy. SQUID-based microtesla MRI for in vivo relaxometry of the human brain. *IEEE Trans. Appl. Supercond.*, 19:823–826, 2009.

[156] P. E. Magnelind, J. J. Gomez, A. N. Matlashov, T. Owens, J. H. Sandin, P. L. Volegov, and M. A. Espy. Co-registration of interleaved MEG and ULF MRI using a 7 channel low-T_c SQUID system. *IEEE Trans. Appl. Supercond.*, 21:456–460, 2011.

[157] A. N. Matlashov, E. Burmistrov, P. E. Magnelind, L. Schultz, A. V. Urbaitis, P. L. Volegov, J. Yoder, and M. A. Espy. SQUID-based systems for co-registration of ultra-low field nuclear magnetic resonance images and magnetoencephalography. *Physica C*, http://dx.doi.org/10.1016/j.physc.2012.04.028, 2012.

[158] J. Pauly, P. Le Roux, D. Nishimura, and A. Macowski. Parameter relations for the Shinnar–Le Roux selective excitation pulse design algorithm. *IEEE Trans. Med. Imaging*, 10:53–65, 1991.

[159] M. A. Janich, R. F. Schulte, M. Schwaiger, and S. J. Glaser. Robust slice-selective broadband refocusing pulses. *J. Magn. Reson.*, 213:126–135, 2011.

[160] J. M. Millar, A. M. Thayer, A. Bielecki, D. B. Zax, and A. Pines. Zero field NMR and NQR with selective pulses and indirect detection. *J. Chem. Phys.*, 83:934–938, 1985.

[161] M. Espy, M. Flynn, J. Gomez, C. Hanson, R. Kraus, P. Magnelind, K. Maskaly, A. Matlashov, S. Newman, T. Owens, M. Peters, H. Sandin, I. Savukov, L. Schultz, A. Urbaitis, P. Volegov, and V. Zotev. Ultra-low field MRI for the detection of liquid explosives. *Supercond. Sci. Technol.*, 23:034023, 2010.

[162] J. Bodurka, A. Jesmanowicz, J. S. Hyde, H. Xu, L. Estkowski, and S.-J. Li. Current-induced magnetic resonance phase imaging. *J. Magn. Reson.*, 137:265–271, 1999.

[163] J. Bodurka and P. A. Bandettini. Toward direct mapping of neuronal activity: MRI detection of ultraweak, transient magnetic field changes. *Magn. Reson. Med.*, 47:1052–1058, 2002.

[164] R. H. Kraus, Jr., M. A. Espy, P. L. Volegov, A. N. Matlachov, J. C. Mosher, A. V. Urbaitis, and V. S. Zotev. Toward SQUID-based direct measurement of neural currents by nuclear magnetic resonance. *IEEE Trans. Appl. Supercond.*, 17:854–857, 2007.

[165] R. H. Kraus, Jr., P. Volegov, A. Matlachov, and M. Espy. Toward direct neural current imaging by resonant mechanisms at ultra-low field. *NeuroImage*, 39:310–317, 2008.

[166] M. Burghoff, H. H. Albrecht, S. Hartwig, I. Hilschenz, R. Körber, T. Sander Thömmes, H. J. Scheer, J. Voigt, and L. Trahms. SQUID system for MEG and low field magnetic resonance. *Metrol. Meas. Syst.*, 16:371–375, 2009.

[167] M. Burghoff, S. Hartwig, A. Cassará, and L. Trahms. Approaches to detect neuronal currents using a DC-mechanism by means of low field magnetic resonance. In *World Congress on Medical Physics and Biomedical Engineering, September 7 – 12, 2009, Munich, Germany*, pages 31–33.

[168] M. Burghoff, H. H. Albrecht, S. Hartwig, I. Hilschenz, R. Körber, N. Höfner, H.-J. Scheer, J. Voigt, L. Trahms, and G. Curio. On the feasibility of neurocurrent imaging by low-field nuclear magnetic resonance. *Appl. Phys. Lett.*, 96:233701, 2010.

[169] N. Höfner, H.-H. Albrecht, A. M. Cassará, G. Curio, S. Hartwig, J. Haueisen, I. Hilschenz, R. Körber, S. Martens, H.-J. Scheer, J. Voigt, L. Trahms, and M. Burghoff. Are brain currents detectable by means of low-field NMR? A phantom study. *Magn. Reson. Imaging*, 29:1365–1373, 2011.

[170] J. W. Belliveau, D. N. Kennedy, Jr., R. C. McKinstry, B. R. Buchbinder, R. M. Weisskoff, M. S. Cohen, J. M. Vevea, T. J. Brady, and B. R. Rosen. Functional mapping of the human visual cortex by magnetic resonance imaging. *Science*, 254:716–719, 1991.

[171] D. Cohen. Magnetoencephalography: Evidence of magnetic fields produced by alpha-rhythm currents. *Science*, 161:784–786, 1968.

[172] D. Cohen. Magnetoencephalography: Detection of the brain's electrical activity with a superconducting magnetometer. *Science*, 175:664–666, 1972.

[173] Y. Zhang, Y. Tavrin, M. Mück, A. I. Braginski, C. Heiden, S. Hampson, C. Pantev, and T. Elbert. Magnetoencephalography using high temperature rf SQUIDs. *Brain Topogr.*, 5:379–382, 1993.

[174] M. S. Dilario, K.-Y. Yang, and S. Yoshizumi. Biomagnetic measurements using low-noise integrated SQUID magnetometers operating in liquid nitrogen. *Appl. Phys. Lett.*, 67:1926–1928, 1995.

[175] D. Drung, F. Ludwig, W. Müller, U. Steinhoff, L. Trahms, H. Koch, Y. Q. Shen, M. B. Jensen, P. Vase, T. Holst, T. Freltoft, and G. Curio. Integrated $YBa_2Cu_3O_{7-x}$ magnetometer for biomagnetic measurements. *Appl. Phys. Lett.*, 68:1421–1423, 1996.

[176] H.-J. Barthelmess, M. Halverscheid, B. Schiefenhövel, E. Heim, M. Schilling, and R. Zimmermann. Low-noise biomagnetic measurements with a multichannel dc-SQUID system at 77 K. *IEEE Trans. Appl. Supercond.*, 11:657–660, 2001.

[177] F. Öisjöen, J. F. Schneiderman, G. A. Figueras, M. L. Chukharkin, A. Kalabukhov, A. Hedström, M. Elam, and D. Winkler. High-T_c superconducting quantum interference device recordings of spontaneous brain activity: Towards high-T_c magnetoencephalography. *Appl. Phys. Lett.*, 100:132601, 2012.

[178] H. Xia, A. Ben-Amar Baranga, D. Hoffman, and M. V. Romalis. Magnetoencephalography with an atomic magnetometer. *Appl. Phys. Lett.*, 89:211104, 2006.

[179] C. Johnson, P. D. D. Schwindt, and M. Weisend. Magnetoencephalography with a two-color pump-probe, fiber-coupled atomic magnetometer. *Appl. Phys. Lett.*, 97:243703, 2010.

[180] T. H. Sander, J. Preusser, R. Mhaskar, J. Kitching, L. Trahms, and S. Knappe. Magnetoencephalography with a chip-scale atomic magnetometer. *Biomed. Opt. Express*, 3:981–990, 2012.

[181] J. Nenonen, S. Taulu, M. Kajola, and A. Ahonen. Total information extracted from MEG measurements. *Int. Congr. Ser.*, 1300:245–248, 2007.

[182] J. C. Mosher, P. S. Lewis, and R. M. Leahy. Multiple dipole modeling and localization from spatio-temporal MEG data. *IEEE Trans. Biomed. Eng.*, 39:541–557, 1992.

[183] D. F. Rose, P. D. Smith, and S. Sato. Magnetoencephalography and epilepsy research. *Science*, 238:329–335, 1987.

[184] J. P. Mäkelä, N. Forss, J. Jääskeläinen, E. Kirveskari, A. Korvenoja, and R. Paetau. Magnetoencephalography in neurosurgery. *Neurosurgery*, 59:493–510, 2006.

[185] P. E. Valk, D. L. Bailey, D. W. Townsend, and M. N. Maisey. *Positron Emission Tomography: Basic Science and Clinical Practice*. Springer-Verlag, London, UK, 2003.

[186] A. P. Gibson, J. C. Hebden, and S. R. Arridge. Recent advances in diffuse optical imaging. *Phys. Med. Biol.*, 50:R1–R43, 2005.

[187] S. Ogawa, R. S. Menon, D. W. Tank, S.-G. Kim, H. Merkle, J. M. Ellermann, and K. Ugurbilt. Functional brain mapping by blood oxygenation level-dependent contrast magnetic resonance imaging. A comparison of signal characteristics with a biophysical model. *Biophys. J.*, 64:803–812, 1993.

[188] M. Burghoff, S. Hartwig, W. Kilian, A. Vorwerk, and L. Trahms. SQUID systems adapted to record nuclear magnetism in low magnetic fields. *IEEE Trans. Appl. Supercond.*, 17:846–849, 2007.

[189] C. W. Crawford, S. Xu, E. J. Siegel, D. Budker, and A. Pines. Fluid-flow characterization with nuclear spins without magnetic resonance. *Appl. Phys. Lett.*, 93:092507, 2008.

[190] R. Jurgons, C. Seliger, A. Hilpert, L. Trahms, S. Odenbach, and C. Alexiou. Drug loaded magnetic nanoparticles for cancer therapy. *J. Phys. Cond. Matter*, 18:S2893–S2902, 2006.

[191] E. Romanus, M. Hückel, C. Groß, S. Prass, W. Weitschies, R. Bräuer, and P. Weber. Magnetic nanoparticle relaxation measurement as a novel tool for in vivo diagnostics. *J. Magn. Magn. Mater.*, 252:387–389, 2002.

[192] Y.-C. Hsu, P. T. Vesanen, J. O. Nieminen, K. C. J. Zevenhoven, J. Dabek, I-L. Chern, R. J. Ilmoniemi, and F.-H. Lin. Efficient concomitant field artifacts reduction using a hybrid space-frequency domain formulism. In *Proceedings of the 20th Annual Meeting of ISMRM, Melbourne, Australia*, page 2474, 2012.

[193] G. M. Bydder and I. R. Young. MR imaging: Clinical use of the inversion recovery sequence. *J. Comput. Assist. Tomogr.*, 9:659–675, 1985.

[194] G. M. Bydder, R. E. Steiner, and L. H. Blumgart. MR imaging of the liver using short TI inversion recovery. *J. Comput. Assist. Tomogr.*, 9:1084–1089, 1985.

[195] P. Mansfield and B. Chapman. Active magnetic screening of coils for static and time-dependent magnetic field generation in NMR imaging. *J. Phys. E: Sci. Instrum.*, 19:540–545, 1986.

[196] P. B. Roemer and S. Hickey. Self-shielded gradient coils for nuclear magnetic resonance imaging. US Patent No. 4,737,716, 1986.

[197] R. Turner and R. M. Bowley. Passive screening of switched magnetic field gradients. *J. Phys. E: Sci. Instrum.*, 19:876–879, 1986.

[198] K. Yoda. Analytical design method of self-shielded planar coils. *J. Appl. Phys.*, 67:4349–4353, 1990.

[199] S. Kakugawa, N. Hino, A. Komura, M. Kitamura, H. Takeshima, T. Yatsuo, and H. Tazaki. Shielding stray magnetic fields of open high field MRI magnets. *IEEE Trans. Appl. Supercond.*, 14:1639–1642, 2004.

[200] M. Kitamura, S. Kakugawa, and K. Maki. An optimal design of coaxial coils with constraints on inner and outer multipole magnetic fields. *IEEE Trans. Appl. Supercond.*, 14:1862–1865, 2004.

[201] K. Zevenhoven and R. J. Ilmoniemi. Performance of SQUID sensor arrays for MRI of the brain. In *Proceedings of the 19th Annual Meeting of ISMRM, Montreal, Canada*, page 4226, 2011.

Aalto-DD 71/2012

ISBN 978-952-60-4644-0
ISBN 978-952-60-4645-7 (pdf)
ISSN-L 1799-4934
ISSN 1799-4934
ISSN 1799-4942 (pdf)

Aalto University
School of Science
Department of Biomedical Engineering and Computational Science

BUSINESS +
ECONOMY

ART +
DESIGN +
ARCHITECTURE

SCIENCE +
TECHNOLOGY

CROSSOVER

DOCTORAL DISSERTATIONS